MicroRNA-32 expression and effects in mouse prostate

Samuli Hartikainen

Master's thesis

Faculty of Medicine and Life Sciences

University of Tampere

21.03.2018

PRO GRADU –TUTKIELMA

Paikka: Tampereen yliopisto, Lääketieteen ja biotieteiden tiedekunta
Tekijä: Hartikainen, Samuli Antti

Otsikko: Mikro-RNA-32:n ilmentyminen hiiren eturauhasessa

Sivut: 72 sivua sekä 6 sivua liitteitä
Ohjaajat: Dosentti Leena Latonen ja professori Tapio Visakorpi
Tarkastajat: Dosentti Leena Latonen ja apulaisprofessori Vesa Hytönen
Aika: 21.03.2018

Tiivistelmä

Tutkimuksen tausta ja tavoitteet: Eturauhassyöpä on kolmanneksi yleisin syöpään liittyvä kuolinsyy länsimaissa. Esimerkiksi Suomessa on diagnosoitu 2010-luvulla noin 5000 uutta eturauhassyöpätapausta joka vuosi. Eturauhassyöpä havaitaan nykyisin useimmin kasvaneen PSA-pitoisuuden myötä verinäytteestä. Laajalle populaatiolle toteutettavassa PSA-tason seurannassa on kuitenkin myös haittoja, ja tämän vuoksi edelleen etsitään parempia tapoja havaita ja erottaa pahanlaatuinen eturauhassyöpä. Esimerkiksi MikroRNA-32:n poikkeava ilmentymistaso voisi tulevaisuudessa olla yksi monista mahdollisista syövän tuntomerkeistä eli markkereista, sillä sen tiedetään olevan eri tasolla pitkälle edenneessä eturauhassyövässä verrattuna eturauhasen hyvänlaatuisen liikakasvun tilanteeseen. Tämän tutkimuksen tavoitteena oli kerätä tietoa mikroRNA-32:n ilmentymisestä ja vaikutuksista eturauhasen eri lohkoissa eri hiirimallien avulla. Hiirimallilla kerättyä tietoa voidaan käyttää esimerkiksi suunnitellessa jatkotutkimuksia ihmisen eturauhasen osalta.

Tutkimusmenetelmät: Käyttämällä tarkkaan valittuja primäärivasta-aineita immunohistokemiallisissa näytevärjäyksissä, pystyttiin näytteistä määrittämään, onko näytesoluissa meneillään esimerkiksi proliferaatio-, mitoosi- tai apoptoosivaihe. Vaikutusten analysointiin käytettiin eri genotyyppejä (villityyppi, PTEN-heterotsygootti, Myc-onkogeeniä ilmentävä, mikroRNA-32:ta ilmentävä), jotka toimivat erilaisten eturauhassyöpävaiheiden mallina. PTEN-heterotsygootteja, 10–11 kuukauden ikäisiä hiiriä käytettiin mallintamaan hyvänlaatuisen kasvaimen eli epiteelikudoksensisäisen neoplasian tilannetta. Kolmen kuukauden ikäistä, Myc-geeniä yliekspressoivaa hiirimallia puolestaan käytettiin aggressiivisemman, primäärisen eturauhassyövän mallina. Normaaliepiteeliä analysoitiin kolmen ja kuuden kuukauden ikäisistä hiirinäytteistä. SYBR™ Green -fluoroforiin perustuvaa kvantitatiivista PCR:ää käytettiin varmistamaan Myc-onkogeenin läsnäolo hiirinäytteissä. TaqMan-menetelmää käytettiin mikroRNA-32:n ilmentymisen todentamiseen käytetyssä hiirisukupolvessa.

Tutkimustulokset ja johtopäätökset: MikroRNA-32:n havaittiin ilmentyvän tutkituissa hiiren eturauhasnäytteissä, mutta sillä ei todettu olevan selvää vaikutusta esimerkiksi proliferaatioon, mitoosiin tai apoptoosiprosessiin missään tutkituista hiirimalleista tässä työssä tarkastelluissa aikapisteissä. Myös Myc-geenin ilmentyminen genotyypiltään Myc-positiivisissa hiirinäytteissä vahvistettiin. Normaalitilannetta, hyvänlaatuisia kasvaimia eli neoplasiaa ja primääristä eturauhassyöpää mallintavissa hiirissä havaittiin esimerkiksi, että mitoosimarkkeri P-H3 ilmentyi kaikissa malleissa. Vähin määrä P-H3:a havaittiin normaalieturauhasmallissa, ja eniten mitoottisia tumia voitiin havaita Myc-sarjan eturauhassyöpämallissa. Vaikka tämän tutkimuksen tuloksien perusteella ei pystyttykään osoittamaan merkittäviä miR-32:n vaikutuksia, voidaan tutkimustuloksia käyttää jatkotutkimuksien pohjana. Hiirimalleilla tehdyt tulokset antavat sovellettavaa tietoa erityisesti ihmisen eturauhasen tutkimukseen.

MASTER'S THESIS

Place:	University of Tampere, Faculty of Medicine and Life Sciences
Author:	Hartikainen, Samuli Antti
Title:	MicroRNA-32 expression and effects in mouse prostate
Pages:	72 pages and 6 pages of supplementary material
Supervisors:	Dr. Leena Latonen and Professor Tapio Visakorpi
Reviewers:	Dr. Leena Latonen and Associate Professor Vesa Hytönen
Date:	21.03.2018

Abstract

Background and aims: Prostate cancer is the third most common cancer-related cause of death in developed countries. For example, solely in Finland roughly 5000 new cases of prostate cancer in men have been diagnosed every year during the current decade. A tumor in the prostate is nowadays often detected by increased PSA concentration in blood. However, the PSA-screening has several drawbacks, and additional markers for prostate cancer are therefore constantly searched for. In future, it might be possible to use microRNA-32 as a one of the markers, since it is known to be expressed differently in severe CRPC (castration-resistant prostate cancer) form of the disease compared to the benign form, BPH (benign prostate hyperplasia). The main objective for this thesis was to gather data from miR-32 expression and effects in different lobes of mice prostate by using different disease type models. The information can then be used as basis for further studies on, for example, the human prostate.

Methods: By using selected primary antibodies in immunohistochemistry, the proliferation-, apoptosis- and mitosis status of the samples could be discovered. Different model systems (wild type genotype, PTEN-heterozygous, Myc-expressing, miR-32 expressing) were used to analyze the effects in different tissue contexts. PTEN-heterozygote 10–11-month-old mice were used as a model of slowly developing intraepithelial neoplasia. MYC-gene-overexpressing, 3-month-old mice were used to simulate more aggressive, primary prostate cancer. Normal epithelium was analyzed from mice samples aged three and six months. SYBR™ Green -based qPCR was used to confirm presence of Myc in the mice samples. TaqMan-qPCR was used to confirm miR-32 expression in the used mice generation.

Results and conclusions: MiR-32-was found to be present but not to have any clear effects on, e.g., proliferation, mitosis or apoptosis processes in the different mice models in the age groups studied in this work. Presence of gene Myc was confirmed in samples, which were Myc-positive by genotype. In mice models for the normal state of prostate, for intraepithelial neoplasia and for primary prostate cancer, it was detected that, for example, the mitotic marker P-H3 was present. Amount of P-H3 was lowest in normal epithelium and highest in Myc-positive tissue. This thesis was not able to find out significant effects, but the obtained information will create a basis for possible further studies. Results from experiments with mouse models give applicable information for the research of human prostate.

Acknowledgments

I would like to thank Leena Latonen, Päivi Martikainen, Marja Pirinen, Riina Kylätie, Hanna Selin, Sari Toivola, Jenni Jouppila, Konsta Kukkonen, Joonas Tuominen, Jani Sarin, Henna Sillanpää, Johannes Malkamäki, Tapio Visakorpi and many others for discussions and support during the thesis process. I'm also very thankful for the funding granted by the Molecular Biology of Prostate Cancer group and the Sigrid Jusélius foundation. I would also like to thank open access journals and those who support them.

Table of contents

Abbreviations

miR-32	Micro-RNA-32 (also abbreviated miR32 or miRNA-32)
PSA	Prostate-specific antigen
PCa	Prostate cancer
CRPC	Castration-resistant prostate cancer
BPH	Benign prostate hyperplasia/hypertrophy
AR	Androgen receptor
ARR2PB	Probasin promoter (PB) with two androgen response elements
ARE/ARR	Androgen (receptor) response element
ARBS	Androgen receptor binding site
GR	Genomic rearrangement (of for example AR)
IHC	Immunohistochemistry
IgG	Immunoglobulin G
MAb	Monoclonal antibody
PAb	Polyclonal antibody
PIN	Prostatic intraepithelial neoplasia
DAB	3,3'-diaminobenzidine
HRP	Horseradish peroxidase
PCNA	Proliferating cell nuclear antigen, a sliding DNA clamp
Casp3	Cleaved caspase 3, an apoptotic marker
P-H3	Phosphorylated histone 3, a mitotic marker
P-S6	Phosphorylated ribosomal protein S6, marker of active PI3K/Akt/mTOR-pathway
PI3K	Phosphoinositide 3-kinase (antagonist of PTEN)
PTEN	Phosphatase and tensin homolog, a protein and a gene
mTOR	Target of rapamycin, mammalian system
Ki-67	Protein encoded by gene MKI67, a proliferation marker
VP	Ventral prostate
LP	Lateral prostate
DP	Dorsal prostate
GITC	Guanidine/guanidium thiocyanate
TBE	A buffer containing Tris (base), borate (acid) and EDTA (chelating agent)

TBS-Tween	A buffer with TBS (Tris-buffered saline) and Tween 20 (Polysorbate 20)
qPCR	Quantitative PCR, a PCR reaction which can be followed in real-time
RT	Reverse transcription
Ct	Threshold cycle, the number of the cycle on which threshold is surpassed
SQ-ratio	Ratio of starting quantities
AGE	Agarose gel electrophoresis
RPM	Revolutions per minute
RCF	Relative centrifugal force, also known as G-force
22Rv1	A prostate cancer cell line 22Rv1
PAXgene	A product family for fixation and stabilization of tissues
TaqMan	qPCR assay type which includes the TaqMan probe
β-Actin	Beta-isoform of actin protein
MYC	MYC-gene (a proto-oncogene)
hiMYC	High-level expression system for the gene MYC
BTG2	BTG family member 2, a protein

1. Introduction

Prostate cancer is the third most common cancer-related cause of death in the developed countries (Damber & Aus, 2008). Roughly 5000 new cases of prostate cancer have been found in Finland each year during the current decade (Suomen Syöpärekisteri, 23.09.2016). A tumor in the prostate is nowadays often detected by increased PSA concentration in blood (Damber & Aus, 2008). However, the PSA-screening has several drawbacks, and additional markers for prostate cancer are therefore constantly searched for (Abate-Shen & Shen, 2000). Prostate cancer usually develops over a long time period and its formation by age is so common that in an autopsy study of 60–70-year-old men, two thirds of the men had had a latent prostate cancer (Lilja, Ulmert, & Vickers, 2008). Therefore, there are many men in the screened population who do not benefit from the PSA-screening, because a tumor in the prostate may be symptomless and the men can die of reasons unrelated to prostate cancer (Lilja, Ulmert, & Vickers, 2008).

Prostate cancer can be in a primary form or in an advanced form, which is able to metastasize (Damber & Aus, 2008). Benign prostate hyperplasia (BPH) is a common, but non-life-threatening form of a prostatic tumor (Damber & Aus, 2008). If prostate cancer advances, metastases usually form, for example, in lymph nodes and in bone, as they are easily reached by the blood circulation (Abate-Shen & Shen, 2000; Damber & Aus, 2008). Malignant prostate cancer is often treated with chemical castration, which depletes the amount of androgens present (Abate-Shen & Shen, 2000). Drugs can, for example, in adrenal glands target the conversion of cholesterol into a form, which is a precursor for the final dihydrotestosterone product (Watson, Arora & Sawyer, 2015). Other drugs target directly the androgen receptor in prostatic cells (Watson et al., 2015). However, the prostate cancer quite usually returns as a castration-resistant form (CRPC), which is able to grow in androgen-deprived conditions due to unknown reasons (Damber & Aus, 2008). Changes in, for example, androgen receptor (AR) structure or copy number are suggested to be the reason (Henzler et al., 2016).

MicroRNA-32 (miR-32) is one of the putative markers for advanced prostate cancer, as it is known to be expressed differently in the severe CRPC form of the disease compared to the benign prostate hyperplasia (Jalava et al., 2012). MiR-32 is also known to be regulated by AR (Jalava et al., 2012). The regulatory microRNAs are known to upregulate or downregulate expression of proteins, which are often important checkpoints for progression in certain cellular processes. For example,

downregulation of protein BTG2 by miR32 could lead to increased AR signal, since BTG2 is thought to be the corepressor for AR gene (Jalava et al., 2012).

In this thesis, the miR-32 is studied further. Mice with different genetic backgrounds are used in this study to assess the effect of miR-32 on various cellular processes. For example, the PTEN-heterozygous mice are used as a model of slowly developing prostatic neoplasia and the Myc-overexpressing mice are used as a model of an advanced tumor in the prostate. Several primary antibodies can be selected for experiment so that they recognize proteins, which are markers of specific cellular processes. For example, detecting PCNA protein (proliferating cell nuclear antigen) in a cell's nuclei would mean that the cell is quite likely proliferating. The primary antibodies are used in indirect immunohistochemistry (IHC), and in addition to that method, quantitative PCR is also used to detect presence of the miR-32 and Myc in different samples.

With the help of the selected methods, this thesis is aiming to study the expression and effects of miR-32 in mice prostate. Information about the effects of miR-32 is valuable especially for further research on the field of prostate research.

2. Literature review

2.1 Prostate cancer and PSA

Prostate cancer usually develops over a long time period and it is the third most common cancer-related cause of death in men in developed countries (Damber & Aus, 2008). Prostate-specific antigen (PSA), which can be detected from a blood sample, is often used to screen possible tumors in the prostate, as the PSA level usually correlates with the prostate size and the assumption has been that tumor formation would be the main reason for the increase in prostate size (Abate-Shen & Shen, 2010; Carvalhal et al., 2010; Damber & Aus, 2008).

Most prostatic cells are androgen-dependent, so limiting androgen levels is used as treatment (Damber & Aus, 2008). If prostate cancer is treated with chemical or surgical castration, both tumor size and PSA level in blood usually initially decrease (Carvalhal et al., 2010). However, quite often prostate cancer returns after an interval as an androgen-independent, castration-resistant prostate cancer (CRPC) (Abate-Shen & Shen, 2010; Damber & Aus, 2008). Most tumors relapse to an incurable form within 2 years of the first treatment (Damber & Aus, 2008). If the prostate cancer advances and produces metastases to bone, there is a high probability that the patient will die in the following years due to cancer-related causes (Damber & Aus, 2008). The information about the type of the tissue where metastases occur – e.g., in lymph nodes near prostate versus metastasizing to distant tissues – can be used in prognostics (Damber & Aus, 2008).

Despite the possibility of severe prostate cancer conditions occurring if a malignant tumor is formed in the prostate, there is also quite a high probability that the prostate cancer will go undetected due to almost absent symptoms and the person in question can die of other natural causes before the prostate cancer can even show any detrimental effects to his health (Damber & Aus, 2008). In such case, detection of an increased PSA-level in a screening could lead to treatment or treatment consideration which could only lower the patient's happiness and life quality (Damber & Aus, 2008). Thus, an easy to use, cheap, and a more precise marker alternative to PSA would be a welcome addition to the tool kit of modern medicine. One of the main problems of using the PSA as a marker is that the PSA is a prostate – not prostate cancer – specific antigen (Lilja, Ulmert, & Vickers, 2008). PSA is produced in all types of prostate: in normal prostate, in benign hyperplasia of prostate (BPH) and in malignant stages of prostate cancer (PCa, CRPC, etc.)(Lilja, Ulmert, & Vickers, 2008).

2.2 Anatomy and histology of mouse and human prostates

The mouse prostate consists of several lobes, which are organized in a different way compared to the zones in a human or dog prostate (Oliveira et al., 2016). The mouse prostate also does not spontaneously develop a prostate cancer which could metastasize into the skeletal system (Oliveira

et al., 2016). Still, the mouse prostate is often used as a tool when the biology of the prostate needs to be studied and tens of genetically engineered models for mouse prostate cancer exist (Abate-Shen & Shen, 2010; Oliveira et al., 2016). As shown in Figure 1B, the mouse prostate consists of four major lobes: anterior, dorsal, lateral and ventral lobes (Oliveira et al., 2016). Out of these four, the latter three are studied in this thesis. In contrast to the mouse prostate, the human prostate could be seen as a combination of peripheral zone, central zone, transition zone and a region of non-glandular fibromuscular stroma (see Figure 1A) (Oliveira et al., 2016).

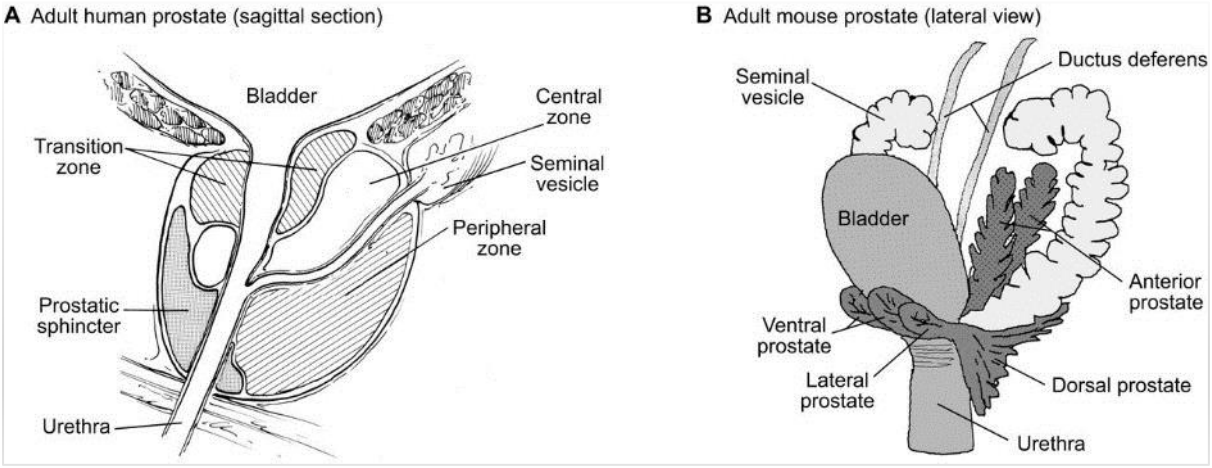

Figure 1. Anatomy of human prostate (left) and mouse prostate (right). Note the location of dorsal, lateral and ventral areas in mouse prostate, which is studied in this thesis. Stroma locations are not specified in the image. Image source (Toivanen & Shen, 2017).

According to some sources (e.g. Oliveira et al., 2016), the peripheral zone of the human prostate can be compared to the dorsolateral area of mouse prostate by their homology in mRNA expression signatures and anatomy, but this view is negated by conclusions from a meeting, which was held specifically to form a consensus opinion on the matter (Shappell et al., 2004). In addition, there are propositions that the central zone could represent the mouse anterior prostate, but there are no proposed counterparts in mouse prostate for the zone, which is located between the peripheral and central zone in human prostate (Oliveira et al., 2016). However, considering that 16 years have passed since the previous consensus meeting in 2001 (Shappell et al., 2004) and that there has been rapid advance in methods in molecular biology in the 21st century (Cameron, Bashor, & Collins, 2014), a precise scrutiny similar to the meeting of 2001 could provide us with new information and help settle the dispute of mouse and human prostate similarity or dissimilarity.

The mouse prostate lobes can usually be distinguished relatively easily by assessing the structure of a hematoxylin and eosin (HE) -stained mouse prostate sample. The ventral lobe usually has very little eosinophilic secretion to the lumen but has some tufting of the epithelium (Oliveira et al., 2016). The lateral lobe is located between dorsal and ventral lobes and it usually has only a few infoldings of the

epithelium (Oliveira et al., 2016). Dorsal lobe has only a little of infolding of the epithelium to the lumen, varying amounts of eosinophilic secretion to the lumen and sometimes stroma surrounding the structure (Oliveira et al., 2016). All three lobe types mentioned above have a gland structure with a lumen in the middle of them (see for example Figure 7). The tissue structure of the prostate is versatile and accordingly, so are the molecular processes in normal and in neoplastic prostates.

2.3 Characteristics of prostate cancer

Primary prostate cancer has relatively low mutational burden compared to other primary cancers such as tumors in bladder, colon or lungs according to The Cancer Genome Atlas data (Robinson et al., 2017). Prostate cancers in primary or metastatic stages also have less immunoinfiltration than many other tissues (Robinson et al., 2017). Immunoinfiltration can be measured to evaluate host tissue immune response, i.e., to discover whether, for example, immunosuppressive or pro-inflammatory cells are present (Robinson et al., 2017). Metastatic prostate cancer cells are also known to frequently contain, i.a., amplifications of the androgen receptor gene, certain gene fusions, mutated p53 gene (also known as TP53) and alterations in the PTEN gene (Wise, Hermida, & Leslie, 2017). Metastatic and castration-resistant prostate cancer could have genetic alterations of the androgen receptor gene in even in 75% of the cases (Henzler et al., 2016), so the genomic sequencing of a patient could be perhaps used in diagnostics together with a hypothetical treatment for a cancer of this stage in the future.

Prostate cells undergo drastic changes in their metabolism during transformation from normal cell to premalignant and later malignant cell (Costello, Franklin, & Feng, 2005). For example, intake and accumulation of zinc is a requirement for metabolism of normal prostate cells, but the cells lose their ability to accumulate zinc in the cancerous stages (Costello et al., 2005). Although debatable, zinc is thought to induce mitochondrial apoptogenesis in certain conditions (Costello et al., 2005). Thus, lower zinc concentration in prostatic cells creates an obstacle for apoptosis, which benefits malignant tumor cells (Costello et al., 2005). The absence of zinc also effectively reverses many metabolic processes, further promoting tumorigenic behavior of the cell as, for example, the altered energy metabolism is often linked to activated oncogenes such as the Myc gene (Costello et al., 2005; Hanahan & Weinberg, 2011).

2.4 Androgen receptor

The androgen receptor (AR) and the signaling pathway linked to it are important factors in the development of a castration-resistant prostate cancer (Jalava et al., 2012). The androgen receptor is a soluble receptor located in either cytosol or the nucleus and it binds dihydrotestosterone, the form into which different androgens are processed (Hu, Wang & Sun, 2017; Watson, Arora & Sawyers,

2015). A treatment used in chemical castration utilizes drug called enzalutamide, which is often able to compete with dihydrotestosterone for the binding site at the androgen receptor (Watson, Arora & Sawyers, 2015). Enzalutamide can also affect androgen receptor by blocking its translocation to nucleus or, and blocking binding to DNA or binding with androgen receptor's cofactors (Watson, Arora & Sawyers, 2015).

The androgen receptor is known to undergo dimerization to bind the DNA strand at androgen response element areas, but it is not confirmed which domains of the androgen receptor are the ones interacting (Hu et al., 2017). In some cases, even a truncated variant protein without the ligand binding domain has been able to bind the DNA (Henzler et al., 2016), so it would seem quite likely that dimerization can be achieved with the DNA-binding domains in the presence of DNA. Also, androgen receptor variants – for example, a normal one (wild type) and a c-terminally truncated one – could pair as a heterodimer and still activate genes in an androgen-deprived cellular condition (Hu et al., 2017). The androgen receptor shares homology with the glucocorticoid receptor, so dimerization with a glucocorticoid receptor could be possible as well, and regulation by this kind of binding has been reported (Hu et al., 2017).

The treatment of malignant prostate cancer often includes chemical castration, which should lower the levels of androgens and therefore also lower the activity of the androgen receptor (Damber & Aus, 2008; Jalava et al., 2012). However, the androgen receptor is apparently able to retain its activity in some cases after the castration, which would suggest that there could be, e.g., alterations in the structure, amount or regulation of the androgen receptors (Jalava et al., 2012).

There are multiple theories to explain the persistent activity of the androgen receptor-related pathways in a situation where the receptor should be almost silent because of the absence of androgens. The copy number of the androgen receptor gene could be amplified (Jalava et al., 2012), the structure of the gene could be rearranged or even truncated by a mutation to, for example, enable transcriptional activity without the androgen-ligand binding domain (Henzler et al., 2016), the translocation from a dormant state at the cytosol to the active regulation in the nucleus could be promoted (Hu et al., 2017), a corepressor for androgen receptor could be instead promoting cancer cell proliferation by downregulating other regulatory proteins (Hu et al., 2017), or the stability of the androgen receptor could be altered by, for example, specific phosphorylation pattern in order to protect it from protein degradation (Hu et al., 2017). Practically, there could be affecting factors in parallel at any step between the very first steps in gene expression activation and the final protein function.

The androgen receptor can promote activation of genes by binding to specific sites (known as androgen binding sites, ARBSs or androgen response elements, AREs) near them (De Bruyn, Bollen, & Claessens, 2011; Jalava et al., 2012). The binding site or element is believed to contain two motifs, such as 5'-AGAACA-3', which are separated by three variable base pairs (De Bruyn et al., 2011). The principle often applies, even though the identification of AREs is not always certain (De Bruyn et al., 2011).

Several genes are known to be activated by androgen receptor binding especially in the castration-resistant prostate cancer cells and some of these genes are protein-coding, but some are also genes for short non-coding RNAs, microRNAs (Jalava et al., 2012). For example, the microRNA-32 is believed to be androgen-binding regulated (Jalava et al., 2012).

2.5 Function of microRNAs and the microRNA-32

MicroRNAs are short, regulatory RNAs, which do not code for proteins (Daniel et al., 2017). MicroRNAs are known to be processed after transcription in several steps, in which longer pre-miRNAs are processed into a shorter form and often also combined with specific proteins of the Argonaute protein family (Daniel et al., 2017). The microRNAs can then function by helping to silence their target gene expression (Daniel et al., 2017).

The processing of miRNAs happens in nucleus and in cytosol (Shen & Hung, 2015). A pri-miR is first cleaved by Drosha ribonuclease and other enzymes in nucleus (Shen & Hung, 2015). The stem-looped pre-miR is further cleaved in cytosol to from the mature microRNA structure, which functions together with RISC proteins (Shen & Hung, 2015). The process can be regulated by different signals; For example, phosphorylation of certain Argonaute proteins leads to decrease in appropriately matured miRNAs, which therefore are not available for RISC complexes (Shen & Hung, 2015). MiRNAs are needed for targeted posttranscriptional gene silencing, so they effect of regulation can be drastic (Shen & Hung, 2015).

MicroRNA-32 from Homo sapiens (hsa-miR-32) was presumably first described in 2001 (Lagos-Quintana et al., 2001) and later studied by many other groups (Jalava et al. 2012, Leite et al., 2011, (Malcomson et al., 2017; Sun et al., 2017). In genome, it has a 70-bp long pre-miR -sequence but it is much shorter – 22 base pairs - in its mature forms (miRBase, 2016).

In previous studies, the human miR-32 has been found to respond to androgen stimulation and reduce apoptosis in vitro (Jalava et al., 2012). The study located an androgen binding site in an intron at about 14 kb distance from the miR-32's intron (Jalava et al., 2012). Also, in another study, the miR-32 has been found to increase proliferation and to have an increased expression in prostate

cancer cell models (Aakula et al., 2015). Together with observations of its effect on protein targets (e.g. BTG2), it was concluded that miR-32 might be an onco-miR and a potential marker for aggressive, CRPC-form of the disease (Jalava et al., 2012). The previously mentioned BTG2 protein was hypothesized to form a feedback loop with the androgen receptor, where an androgen receptor signal would upregulate miR-32, which would downregulate BTG2, which subsequently would lead to upregulation of the androgen receptor, because BTG2 would have been its corepressor (Jalava et al., 2012).

One form of the microRNA-32, the miR-32-5p, has been studied further as a marker of prostate cancer (Daniel et al., 2017). In the study, miR-32-5p level in blood was found to be downregulated in prostate cancer. Therefore, it could be used as a marker but only as a panel together with other markers (Daniel et al., 2017).

In addition to the prostate, effects of the miR-32 have been or are being studied in areas such as brown adipose tissue (Ng et al., 2017), colon tissue (Malcomson et al., 2017), breast cancer cells (Xia et al., 2017) and in lung tissue (Sun et al., 2017). Therefore, miR-32 has been identified as a regulatory micro-RNA in many pathways, including the p38 MAPK pathway, the NF-κB-pathway and the cyclin E-dependent cell cycle regulation (Malcomson et al., 2017; Ng et al., 2017; Xia et al., 2017). As an example of cross-talk between pathways, the NF-κB-pathway is also apoptosis-related (see Figure 4).

But what does the number 32 in the name of miR-32 mean? The miR-32 was 32nd micro-RNA which had been reported in a publication (miRBase, 2016). Because of the sequential numbering, the system is not intuitive: for example, the miR-200 family consists of miR-200a, b and c but also of miR-429 and miR-141 (Liu et al., 2017).

2.6 PTEN

PTEN (Phosphatase and tensin homologue) is a tumor suppressor gene, which regulates many signaling pathways with its phosphatase activity (Di Cristofano et al., 1998). PTEN is one of the most commonly altered genes – by somatic mutations – in all metastatic cancers (Robinson et al., 2017). Loss of PTEN function is also one of the main events in the development of prostate cancer (Wise et al., 2017).

PTEN is a major regulator, especially in the phosphoinositide 3-kinase (PI3K) signaling network, as it antagonizes kinase PI3K (Wise et al., 2017; Song et al., 2012). This way, the most direct effect of PTEN is on the PI3K/AKT/mTOR-pathway (see Figure 2), which is one of the many cell cycle -targeting regulatory systems (Wise et al., 2017). There are several known two-directional negative feedback

mechanisms between the PI3K/PTEN-signaling system and the androgen receptor signaling pathways (Wise et al., 2017). Deactivation of PTEN is linked to a notable activation of PI3K and the androgen receptor pathways, e.g., in aggressive prostate cancer (Wise et al., 2017). PTEN can also directly interact with other tumor suppressors such as p53 (Wise et al., 2017).

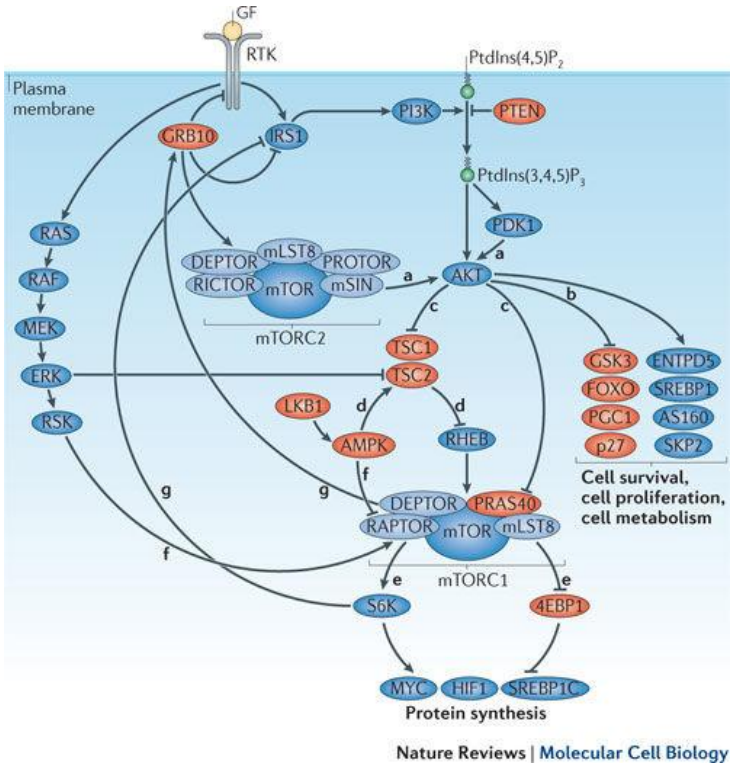

Figure 2. PTEN/PI3K/AKT/mTOR pathway. Note S6K (marked with bolded letter e), which phosphorylates the ribosomal S6 protein. Also, the PTEN and MYC, which were partially absent or present abundantly in different mouse model systems, can be seen as a part of the pathway. Several up- and downregulated targets (bolded letter b) in cell proliferation are listed, even though the Ki-67 or PCNA, which were used as markers in this thesis are not listed (Figure from Song et al., 2012).

Complete inactivation of the PTEN gene will result in embryonic lethality in mammals, and a deletion of one allele in spontaneous development of tumors (Di Cristofano et al., 1998). Nevertheless, mice do not spontaneously develop prostate cancer (Oliveira et al., 2016) and therefore genetically engineered mouse models need to be used in order to study prostate cancer in mice. Therefore, PTEN-heterozygous mice have been used in many prostate cancer studies (Abate-Shen & Shen, 2010).

Mice with a PTEN+/- genotype often form (high-grade) PIN-lesions (prostatic intraepithelial neoplasia), which could be called a precancerous state of prostate (Steven, Lowe, & Young, 2002). PIN-lesions have atypical epithelial cells and large nuclei compared to the cell volume (Steven et al., 2002). High-grade PIN-lesions have the most intraepithelial neoplasia among the PIN-lesions (Steven et al., 2002). The PIN-lesions which originate from the PTEN+/- genotype are not invasive before more mutant traits are introduced, such as the deletion of one allele in the protein 27 gene (p27),

which is shown to produce invasive PIN-lesions (Trotman et al., 2003). The simultaneously PTEN- and p27-mutant mice develop tissue which resembles the human benign prostate hyperplasia (Trotman et al., 2003).

2.7 Myc

MYC is a gene with an important role in transcription regulation, but it is also relatively prone to tumorigenic behavior and is thus often called an oncogene (NCBI, 2017). A viral and a human version of Myc are known, and here Myc refers to the human Myc (c-Myc). The effect of the Myc overexpression can be seen, for example, in the emergence of PIN-lesions or in immortalization of non-tumorigenic prostate cells in humans (Abate-Shen & Shen, 2010) or as an increase in prostate mass and in proliferation of epithelial cells in the prostate (Geng et al., 2017).

There have also been several reports of an effect, where an ever-increasing expression of oncogenes such as Myc would actually lead to apoptosis because the constant signal from an active Myc would trigger a response from the cell (Hanahan & Weinberg, 2011). It is likely, that different observations are not only dependent on Myc (over)expression, but the outcome is dictated by the complex regulatory circuit, where Myc crosstalks with many functional signaling pathways – the complete cellular environment, so to speak (Hanahan & Weinberg, 2011).

MYC can be overexpressed by mutations in genes regulating it, for example, the gene for SPOP protein (Geng et al., 2017), or with expression systems such as the transgenic introduction of the rat probasin promoter, which is accompanied by two androgen-responsive elements (abbreviated ARR2PB)(Abate-Shen & Shen, 2010). The latter system is called hi-Myc or low-Myc depending on the expression level (Abate-Shen & Shen, 2010). The ARR2PB-system is discussed further in the next chapter (2.8).

Depending on the presence other genetic alterations (e.g. for p53 and Pten), the c-Myc mice have had various malignancy stages: there are also reports of mice with benign prostate conditions, but majority of the mice have had microinvasive or fully cancerous conditions in the prostate (Kim et al., 2012). Therefore, in this study, the Myc-overexpressing mice are used as a model of a primary prostate cancer.

2.8 ARR2PB expression system

ARR2PB is a probasin promoter with androgen receptor response elements (Andriani et al., 2001). The system enables activation of a gene downstream from the promotor in the presence of androgen receptors and androgens such as dihydrotestosterone (Andriani et al., 2001). The system has been shown to be activated only in prostatic cells in an androgen-dependent way and similarly,

it has been demonstrated that the AR receptor pathway in non-prostatic cells in the presence of androgen is not activated (Andriani et al., 2001). Also, the ARR2PB-system is not activated in prostatic or non-prostatic cells if they do not have androgens present (Andriani et al., 2001). Thus, ARR2PB was previously chosen to be the promoter system for miR32-expression (see Figure 3) and Myc-gene overexpression in mice used in this study because it only affects the prostate but no other tissues (Ellwood-Yen, 2003; Latonen et al., 2017). Lentiviral-based overexpression systems are also quite often and quite effectively used in similar setups (Liu et al., 2017), but the ARR2PB has the advantage of tissue-specificity (Andriani et al., 2001).

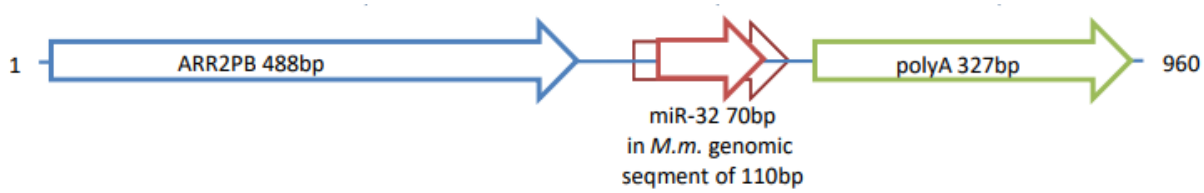

Figure 3. A transgene, where ARR2PB-promoter system is used for miR-32 expression. A poly-A-tail -producing region is also shown. Figure abridged from Latonen (2014).

2.9 Detecting activity of different cellular pathways with IHC

Histology studies organization of the cells into tissues, for example in this case the different structures and types of cells in prostate. With immunohistochemistry, the tissue samples and the cells in them can be fixated – almost as they were in vivo. The current state of the cell can be then analyzed with suitably selected antibodies. The following sections present antibody markers, which can be used to detect apoptosis, proliferation, mitosis and activation of PI3K/AKT/mTOR-pathway with immunohistochemistry. Finding different amount of the studied proteins in different models enables deducing which pathways were active in the samples of each model system.

2.9.1 Apoptotic markers

Caspase-3 is an important enzyme in the apoptosis process (see Figure 4) and a part of caspase protein family (Fulda, 2014). It is cleaving proteolytically other key proteins of the apoptotic cascade such as poly (ADP-ribose) polymerase (PARP), but it is also a target of cleavage itself (Casciola-Rosen et al., 1995; Fulda, 2014). The zymogen form of caspase-3 is kept inactive by inhibitors such as XIAP protein and activated by cleavage only after the inhibitors are inhibited (Fulda, 2014).

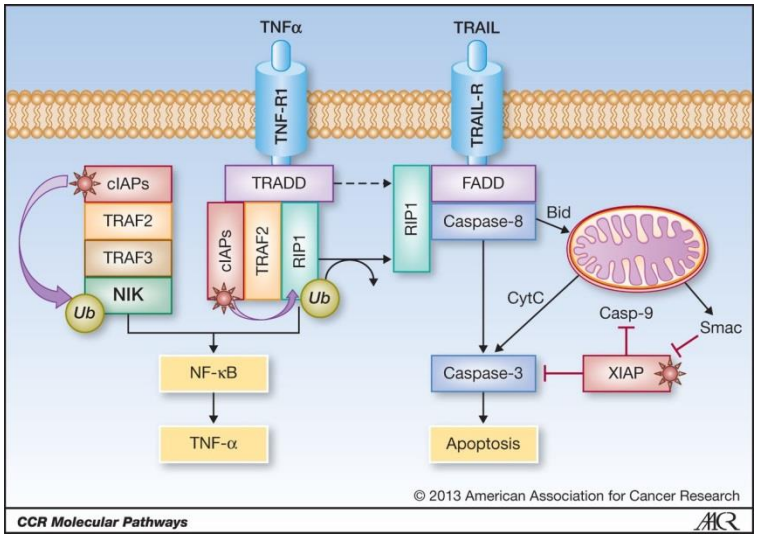

Figure 4. Caspase 3 is part of the apoptosis, the cell death pathway. Activation of caspase 3 requires, for example, cytochrome-c exported from mitochondria to activate it and at the same time the deactivation of the inhibitor XIAP is required. Image is simplified and does not show, e.g., PARP protein (Figure from Fulda, 2014).

Caspase-3 which is cleaved specifically at aspartate 175 is thought to be a signal of an active apoptosis pathway (Fernandes-Alnemri, Litwackt & Alnemri, 1994), since caspase-3 will induce apoptosis if not inhibited (Fulda, 2014). Caspase-3 is also known by names CPP-32 and Apoptain (Casciola-Rosen et al., 1995; Fulda, 2014).

2.9.2 Proliferation markers

PCNA can be used as a marker of proliferation as its name hints (Proliferating cell nuclear antigen) (Juríková et al., 2016). PCNA is a sliding clamp protein that assists in replication of DNA (Juríková et al., 2016). Regulators of cell cycle such as cyclin dependent kinases regulate it for example by binding to PCNA (Juríková et al., 2016). Also, PCNA is a part of the mechanisms for DNA excision repair, assembly of chromatin, cell cycle control and transcription of RNA (Juríková et al., 2016).

The Ki-67 protein is another widely accepted proliferation marker because it is known to be present when the cell is in stages G1, S, G2, or in mitosis (Scholzen & Gerdes, 2000). Respectively, Ki-67 (staining) is absent in the quiescent phase of the cell (Scholzen & Gerdes, 2000) and therefore it has been successfully used in immunohistochemical experiments in many studies (Geng et al., 2017; Liu et al., 2017; Scholzen & Gerdes, 2000). Ki-67 is a non-histone protein in the nucleus and it may be related to the cell cycle progression even though the mechanism is still unknown (Scholzen & Gerdes, 2000).

Used together or alone, PCNA and Ki-67 are quite reliable markers of proliferation. Still, the two do not always correlate to one another (Juríková et al., 2016). A major drawback of the PCNA as a

proliferation marker is that it may be present in cells as a part of repair mechanisms and not as a marker of DNA replication (Juríková et al., 2016).

2.9.3 Mitotic markers

Histone 3 (H3) is one of the four nucleosome core histone proteins and can be modified on its tail like all the other histones (Zhang & Reinberg, 2001). The phosphorylation of histone 3 at its tail region at serine 10 and 28 and at threonine 11 is often correlated with the condensation of the chromosome, which occurs during the early prophase in mitosis (Tapia et al., 2006). Thus, phosphorylated H3 (P-H3) can be used as a mitotic marker (Tapia et al., 2006).

2.9.4 Markers for PI3K/AKT/mTOR-pathway

Phosphorylated S6-protein is yet another commonly used marker in immunohistochemistry (Egervári et al., 2011). The S6-protein is a component of 40S ribosome but also a substrate of the S6-kinase (Magnuson, Ekim, & Fingar, 2012). This way, the S6-protein is related to the PI3K/Akt/mTOR-signaling pathway (mTOR = target of rapamycin, mammalian form, PI3K = phosphoinositide 3-kinase), which integrates signals such as mitogens and growth factors from the cellular environment to inhibit the catabolic and to promote anabolic cellular functions in the cell (Magnuson et al., 2012; Wise et al., 2017). Phosphorylated S6-protein is therefore a marker of active PI3K/Akt/mTOR-pathway.

Protein S6 is regulated by phosphorylation especially at serine 235, 236, 240, 244 and 247 (Magnuson et al., 2012). The consequence of the ribosomal protein S6 phosphorylation is not completely understood, but it has been in some cases to correlate with mitosis (Egervári et al., 2011) and with the increased translation of mRNA transcripts, many of which code proteins, which are involved in the progression of the cell cycle (Magnuson et al., 2012). Some of the mRNAs also encode ribosomal proteins or elongation factors, which are required in the translation process (Magnuson et al., 2012). This way, the active PI3K/Akt/mTOR-pathway might have a direct regulatory role, but the effect might be in some cases independent from the S6 kinases and the P-S6 (Magnuson et al., 2012). Concisely said, the P-S6 is a marker of active PI3K/Akt/mTOR-pathway, but active the pathway does not always appear together with the phosphorylated S6-protein.

2.9.5 Immunohistochemistry

2.9.5.1 Fixation

In immunohistochemistry, the content of the tissue sample's cells is first fixated to preserve the histomorphology and/or the antigenicity for analysis. Depending on the use purpose, the fixative can also be chosen to preserve nucleic acids. Intact histomorphology is often required for pathology

purposes, whereas keeping biomolecules in native form is essential for their more detailed analysis of for example marker proteins and nucleic acid sequence (Kap et al., 2011).

Fixation of the sample with, for example, formalin leads to a partial or complete masking of antigens as the proteins become linked to one another or to nucleic acids (Warford et al., 2014). Therefore, epitope retrieval is needed before the sample can be used for staining.

Retrieval can be done in a protease-induced way or by using heat, but the heat induced epitope retrieval (HIER) is the more common choice for formalin fixed and paraffin embedded samples (FFPEs) if the samples are not freshly fixated (Warford et al., 2014). Heat and a suitable buffer unmask the antigens, but the mechanism is quite poorly understood (Warford et al., 2014).

Fixation of the sample often preserve either the biomolecules in the tissue or only the histology of the sample. A PAXgene®-based storing method has been shown to preserve the biomolecules in a sample quite well because the fixation by PAXgene does not cross-link molecules (Kap et al., 2011). Also, the same study found out that there were no notable differences between the histology of PAXgene- and FFPE-stored samples (Kap et al., 2011). Therefore, PAXgene seems to be a better choice of these two, especially if the sample's DNA, RNA, miRNA, or proteins need to be kept in their native form (Kap et al., 2011).

2.9.5.2 Indirect immunohistochemistry

The basic principle of immunohistochemistry is detecting specific antigens with suitable antibodies and then detecting the bound antibodies with, for example, a chromogenic substance. An example of an indirect immunohistochemistry-technique with two antibodies, an enzyme, and substrates is presented in Figure 5.

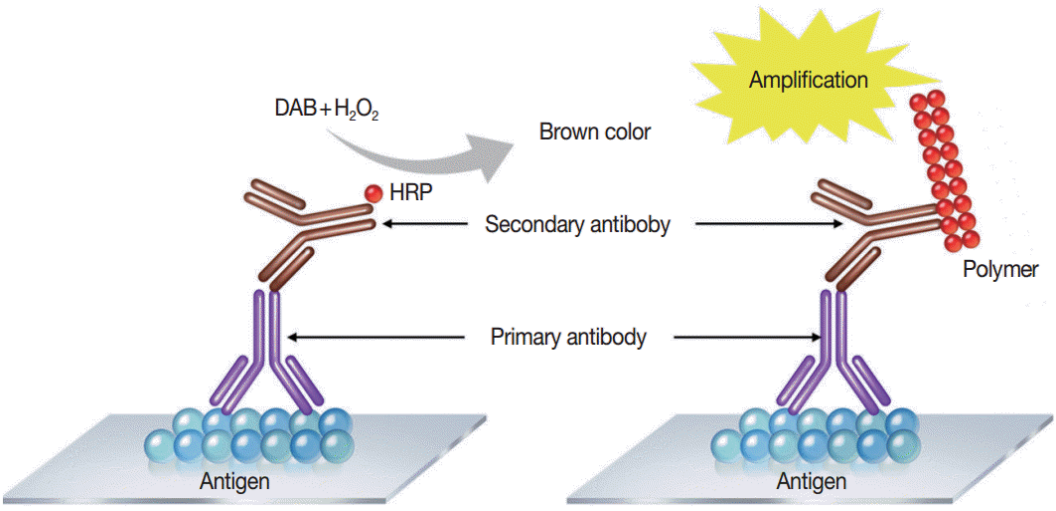

Figure 5. The basic principle of indirect immunohistochemistry. Staining with primary and secondary antibodies gives the specificity, and the horseradish peroxidase (HRP) together with the chromogenic DAB

(diaminobenzidine) and the substrate (H_2O_2) produces the brown color, which is amplified during an incubation period. Image from (Kim, Roh, & Park, 2016).

Monoclonal antibodies (Mab) recognize specific epitopes on the antigen. For example, in this thesis, a monoclonal antibody was used to detect specific phosphorylated sites at the histone H3 tail. The ability of monoclonal antibodies to bind to a certain epitope is at the same time a great advantage but also poses a threat; a change in the epitope structure (because of glycosylation, for example) may prevent recognition (Lipman et al., 2005). Polyclonal antibodies (PAb) recognize many epitopes as they are more heterogeneous (Lipman et al., 2005). They are also more stable and withstand more varying in the pH level than the monoclonal antibodies (Lipman et al., 2005).

In indirect immunohistochemistry, the secondary antibody must be produced so that it is targeted against the immunoglobulins of the same species, in which the primary antibody had been produced (Lipman et al., 2005). The main benefit of this approach is that the primary antibody can be specific to a wanted, unique epitope on an antigen and simultaneously, a generic, reporter-molecule-binding secondary antibody can be used (Lipman et al., 2005).

Indirect immunohistochemistry can be applied with, for example, polymer-based detection techniques such as the HRP/DAB-pair (see Figure 5). The horseradish peroxidase is an enzyme which can produce a brown color in a reaction where it catalyzes 3,3'-diaminobenzidine in the presence of H_20_2 (Kim et al., 2016). However, as a drawback, a too strong H_20_2 -concentration could destroy some antigens such as the CD4-glycoprotein (Kim et al., 2016). Hematoxylin can be used as an auxiliary stain, so that previously unstained cells will be stained blue. HRP/DAB activity lasts only about 10 minutes (Warford et al., 2014), which is a relatively short time compared to other alternative enzymes but often more than sufficient to produce a detectable amount of brown stain, as the color reaction is amplified by polymerization (Kim et al., 2016).

2.10 RNA extraction and cDNA synthesis with reverse transcription

The RNA extraction methods depend on the strategy which has been used to store the sample. PAXgene® is a relatively new way of storing the sample, and specific protocols are made for it. A traditional alternative RNA isolation technique utilizes Trizol-chloroform-extraction. The two methods have been found to be similar in extraction quality and yield (Remáková, 2013). PAXgene preserves both the histology and the biomolecules of the sample, which is useful, especially in cases where, for example, immunohistochemistry and RNA isolation need be done using the same samples (Kap, 2011). Reverse transcription can then be performed from isolated RNA extracts, with reverse transcriptase enzymes to synthesize cDNA. The cDNA is the main source material for RT-qPCR.

2.11 qPCR with SYBR™ Green

The quantitative PCR with SYBR™ Green -method utilizes the ability of the SYBR Green -fluorophore to bind to the minor groove of the double stranded DNA. The amount of the dsDNA is detected at the annealing phase of qPCR cycle. Also, the temperature at which the DNA strands separate from each other (denaturation, loss of signal) on average can be determined, when a melt curve step is programmed to the ending of the qPCR process. Two types of graphs can be then obtained: one is formed by comparing fluorescence signal and temperature, and the other graph by comparing the change of these two to the temperature.

One major disadvantage of the SYBR™ green is its ability to bind unspecifically to all dsDNA. However, with several different graphs (melt curve, melt peak etc.), the user can distinguish whether a contaminant is present or just the intended PCR product (Thermo Fisher Scientific Inc., 2015). In this study, the qPCR with SYBR Green was used for genotyping the samples to confirm the presence of Myc-gene, which was expressed with the ARR2PB-promoter system.

2.12 qPCR with the TaqMan® assay

The TaqMan® assay is especially suitable for microRNAs thanks to the technique's high signal-to-noise ratio (Applied Biosystems, 2006). First step in TaqMan assay is the reverse transcription of miRNA into cDNA. When the cDNA is used in the TaqMan® -based qPCR, the TaqMan® probe anneals specifically to a complementary sequence between the forward and reverse primer sites. The probe (see Figure 6) has a quencher and a reporter, which is cleaved out after polymerization and strand displacement.

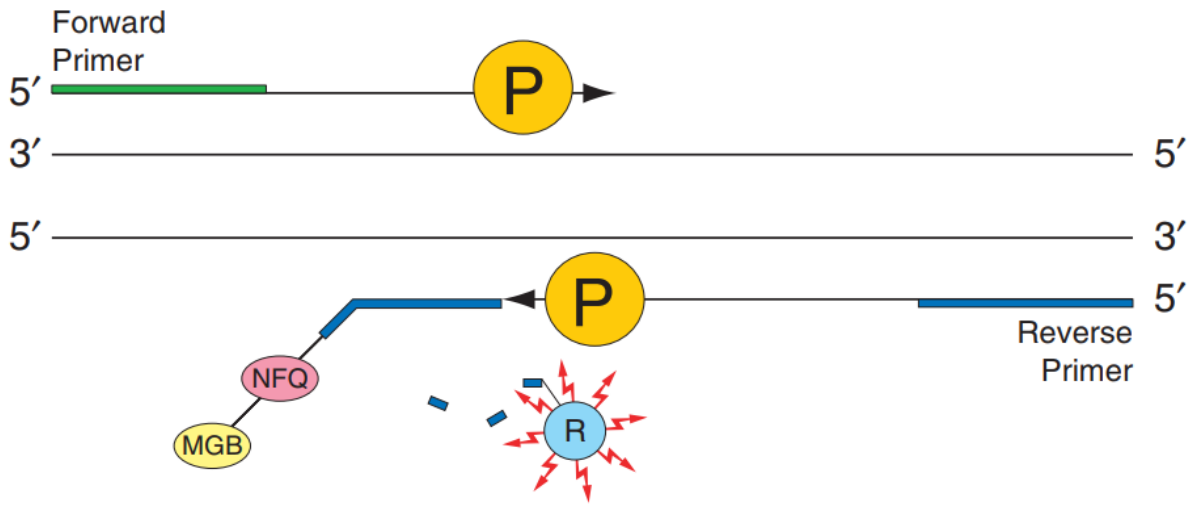

Figure 6. TaqMan® probe at strand displacement stage. The probe has an area (in blue) complementary to the cDNA sequence, quenchers (NFQ and MGB) and a reporter (marked with letter R). The cleavage of the reporter

enables fluorescent signal due to the loss of proximity of the quencher. Also, the forward and reverse primers and the polymerase (P) are shown. Image modified from Applied Biosystems (2006).

The cleavage means that the reporter-part of the probe is no longer in the proximity of the quencher, and therefore it emits fluorescent signal, which can be detected. The reporter can be, for example, fluorescein amidite (FAM) and its derivatives (Applied Biosystems, 2006). One of the major advantages of the TaqMan® assay technique is its specificity to the sequence and thus specific cDNA can be amplified (Applied Biosystems, 2006).

In this study, the TaqMan-qPCR was applied in genotyping miR-32 in the samples. The previously introduced SYBR-dye would not be applicable to miRNA expression studies, since the dye molecule binds to at least 20 bp long dsDNA segment, and therefore a 22 nucleotides long miRNA would be almost completely bound by the dye (Wang et al., 2010). An effect of this could be the distortion of the fluorescent signal in the miRNA sample population (Wang et al., 2010).

3. Objectives

MiR-32 functions in mouse prostate are still relatively poorly known, and more information is required especially about the effect of miR-32 for different malignancy stages of prostatic neoplasia and tumors. The objective of this thesis was therefore to gather data from miR-32 expression and effects in different lobes of prostate in different mouse models.

By using selected primary antibodies in immunohistochemistry, the proliferation-, apoptosis- and mitosis status could be discovered. Also, the activity of PI3K/Akt/mTOR-pathway was studied. Different model systems (wild type genotype, PTEN-heterozygous, Myc-expressing, miR-32 expressing) with different age groups were used to analyze the effects in different tissue context. The SYBR™ Green -based qPCR was used to confirm the presence of Myc in the mice samples. The TaqMan-qPCR was used to confirm the functionality of the ARR2PB-miR-32 transgene, i.e., the presence of the miR-32 in the used mice generations.

4. Materials and methods

4.1 Samples series for IHC staining experiments

4.1.1 MiR-32-series: analysis of normal epithelium

This sample series had mice of 3–6 months of age with wild type genotype or with miR-32 expression by ARR2PB-miR-32. Thus, the series gave information about the normal state and the effect of miR-32 in these conditions. For each of the sets for the four antibodies, there were 16 pre-mounted sample slides from 12 different mice with miR-32+/- genotype (see supplementary Table 3 for the sample list).

4.1.2 PTEN/miR-32-series: neoplasia model

The samples in the PTEN-series were representing neoplasia conditions. The samples were from 12 different mice of 10-11 months of age and with Pten+/- miR-32+/- genotype (see supplementary Table 3 for the sample list). Four tissue samples had been selected from each mouse so that they were in close proximity of each other in the dissected tissue and contained high-grade-PIN-lesions. These pre-mounted samples per mice were then used to study the tissue.

4.1.3 Myc/miR-32-series: primary prostate cancer model

The Myc/miR-32 sample series served as a model of a primary prostate cancer in this study. The samples were from 20 individual mice with Myc+/- miR-32 +/- genotype (see supplementary Table 3 for the sample list). The Myc-overexpressing hi-Myc-mice were 3 months old.

4.2 Immunohistochemistry protocol and antibodies

4.2.1 Immunohistochemistry protocol

The protocol for immunohistochemistry had been previously optimized for similar use (Alanen, 2014). As the first step, deparaffinization was done by submerging the samples twice in n-hexane liquid for three minutes and twice in absolute ethanol for two minutes. The samples were air dried in a hood. The antigen retrieval phase was done with a LabVision PT Module, in which two different buffers were used; pH 6 (10 mM with 0,05 % Tween 20) and pH 9 (10 mM Tris and 1 mM EDTA). The used buffer was heated to +98°C temperature and samples boiled in it for 15 minutes. After cooling, sample slides were moved to 1 x TBS-Tween liquid and from there to a LabVision Autostainer 480 device for the staining program. There were three different Autostainer-machines to use: the chosen and used Autostainer device was the most modern model, from the year 2004.

The staining program was manually set as follows; A wash with 1xTBS-Tween. Applying of endogenous peroxidase blocking liquid, 3% H_20_2 on samples for five minutes. Another wash with

1xTBS-Tween. Primary antibody solution was left for 30 minutes on samples before unattached antibodies were washed away with 1xTBS-Tween. Secondary antibody, the N-Histofine Simple Stain MAX PO Multi (Nichirei Bioscience), was given 30 minutes to attach to the primary antibodies. Unattached molecules were washed away with 1xTBS-Tween and after this the ImmPACT DAB peroxidase substrate (with 15 µl of DAB chromogen and 1ml of DAB diluent) was applied for five minutes. Slides were washed with dH_20 and 1xTBS-Tween. Unfiltered Mayer's hematoxylin was applied for two minutes. Slides were washed once again with 1xTBS-Tween and dH_20.

Sample slides were placed in following set of solutions in preparation for cover glass placement; dH_20 for two minutes, 70% ethanol, 94% ethanol and absolute ethanol each for two minutes and xylene twice for two minutes. After this, a Dako Coverslipper device was used to place glass coverslips for the slides.

For testing purposes, two samples were stained with an Akt-targeting antibody and one more with a Ki-67-targeting antibody. Second time, the protocol was carried out identically to the previous staining procedure, except the two dH_20 wash phases were discarded.

4.2.2 Primary antibodies

The used primary antibodies were against PCNA (dilution 1:5000, Cell Signaling Technology, mouse monoclonal antibody #2586S), against S6 protein phosphorylated at S235 and S236 (1:500, CST, antibody purified from polyclonal antibodies, #2211S, cytoplasmic marker), against histone 3 phosphorylated at serine 10 (1:250, CST, antibody purified from polyclonal antibodies, #9701S), and against cleaved caspase 3 (1:250, CST, Rabbit monoclonal antibody, which recognizes only caspase 3 cleaved at Asp175, #9579). In the optimation phase and with Myc/miR-32-series, Ki-67 antibody (Thermo Fisher, rabbit monoclonal SP6-antibody) was used in dilution ratio 1:100. During the first testing phase, Akt-protein-targeting antibodies (a-P-akt S473 (D9E) Mouse IgG in 1:140 dilution and a-Pan-akt (40D4) Rabbit IgG in dilution 1:250) were used as primary antibodies to stain the samples. Antibodies were diluted with normal antibody diluent.

4.3 Scanning of the stained sample slides

Scanning was performed with a virtual whole slide scanning system at the university's Imagining Core Facility. The scanner system had an Olympus BX43 microscope system with a PL200 slide mover system by JiLab and an Objective Imaging Surveyor (Objective Imaging Ltd) software. A 10x (for normal epithelium and neoplasia samples) and 20x (for the primary prostate cancer model set) magnification was used in the optical pathway. Depending on the series, either the whole set was scanned with one focusing distance or the distance was set for each slide separately.

4.4 Quantifying images of IHC-stained slides

Quantification of most of the sample images was done by analyzing scanned images with the JVSview software (http://jvsmicroscope.uta.fi/?q=jvsview) and with the ImageJ software (https://imagej.nih.gov/ij/). A view with 40x magnification was obtained from the JVSview and then quantified in the ImageJ with the Cell counter -plugin (https://imagej.nih.gov/ij/plugins/cell-counter.html). Cell counter enables marking each stained nucleus with a colored marker. Depending on the antibody, different categories for sorting and counting nuclei were used. After this, data was collected for data analysis.

At least 500 nuclei were counted per sample when the antibody was staining nuclei. For whole-cell-staining P-S6, no fixed number of evaluated cells was used but instead a representative sample area for each sample was estimated. Quantifying was done every time without knowing the genotype of each sample. Out of the three sample sections on a slide, the most average one was selected each time.

4.4.1 Mitotic marker

Mitotic marker P-H3 was assessed by comparing blue and brown-stained nuclei.

4.4.2 Proliferation markers

Analysis of the proliferation marker PCNA for all sample types was done by using four color categories: dark brown, medium brown, weak brown and blue. The staining by another nucleic proliferation marker, Ki-67, was categorized into brown and blue groups.

4.4.3 Apoptosis marker

Analysis of the apoptosis marker cleaved caspase-3 was done by using a binary category system; nuclei were either labeled as brown or blue.

4.4.4 Marker for PI3K/Akt/mTOR-pathway

To find the most reliable and suitable method for the cytosolic P-S6-staining quantification (where individual nuclei cannot be counted), multiple methods were sought. Various approaches for quantification of P-S6 staining had been previously used. At the best, these methods were only semiquantitative as one would expect with immunohistochemistry.

In the method used here for normal epithelium samples, and previously by de Vicente et al. (2017), the slides were observed and sorted into categories of less than 10% of positive cells, 10%–50% of positive cells, or more than 50% positive cells. The sample slides were viewed without knowing the genotype of the samples. Additionally, the data was dichotomized into P-S6 expressing (more than 10% of the cells stained) and into P-S6 negative (less than 10% cells stained) group.

The samples from neoplasia model mice were analyzed with another system. Instead of evaluation of the stained area, a web-based software ImmunoRatio (jvsmicroscope.uta.fi/immunoratio/) was used to quantify the amount of brown stain present in each slide.

The ImmunoRatio software is designed for analysis of nuclei stained with DAB and hematoxylin, but it seemed to analyze quite well the whole cell area with a slightly modified setting. The image scale (pixels/µm) was set as 1,0 and the images were saturated before the ImmunoRatio-analysis by +100 units in paint.net-software (dotPDN LLC.). The adjustment was performed for all images in the same way. The reason for saturation was to achieve the most realistic result – without the saturation, large areas of brown stain would have gone undetected. The PIN-lesions from the sample images were cropped out of the background so that the ImmunoRatio-analyzed images contained only the PIN-lesion. To reduce the effect of non-specific staining, secreted matter from luminal space inside the lesion was also removed from each image.

4.5 RNA extraction

Samples used here were stored frozen and had the Myc+/- miR32 +/- genotype. The RNA extraction from these PAXgene-stored tissue samples was performed with the PreAnalytix PAXgene® Tissue RNA Kit (PreAnalytiX GmbH, Switzerland) according to the manufacturer's guide (see supplements 9.2). The volume of the extracted product was set to 20µl for every sample. The purity of the RNA extraction product was analyzed each time with a Nanodrop 2000 device (Thermo Fisher Scientific), which measures absorbance at several wavelengths.

4.6 cDNA synthesis

For reverse transcription reaction, all the samples were diluted so that a suitable volume containing 100 ng of the sample was obtained. The template RNA (100 ng) was mixed with 0,5 µl of a random hexamer primer (c = 0,2µg/µl, Thermo Fisher Scientific) and nuclease-free water was added so that the volume was 13 µl for each sample. The samples were incubated in +65°C for five minutes and chilled on ice. 4 µl of 5xRT-buffer (Thermo Fisher Scientific) and 2 µl of 10 mM dNTP-mix (Thermo Fisher Scientific) were added to each sample. Also, 0,5 µl of the Ribolock RNase (Thermo Fisher Scientific) and 0,5 µl of the SuperScript IV (a RT enzyme, Thermo Fisher Scientific) were added to each sample. The PCR step consisted of a 10-minute incubation in 25°C, 30 min in 50°C, and 5 min in 85°C. All cDNA samples were diluted 1:20 and stored in Eppendorf-tubes in a -20°C freezer.

4.7 qPCR and data-analysis

For each sample and standard, two contemporaneous samples were made to better detect outliers. The master mix for all qPCR consisted of 0,1 µl of the forward primer and 0,1 µl of the reverse primer, 10 µl of the Maxima SYBR Green mix (Thermo Fisher Scientific) and 7,8 µl of nuclease-free

water (Thermo Fisher Scientific) per sample. The Master mix was made for a few more samples than what was needed. 18 µl of master mix and 2 µl of sample or standard or non-template control was pipetted into a well in a 96-well plate. The well plate was sealed with a Bio-Rad Microseal B Adhesive sealer and centrifuged with a counterweight for 1 min with 800 g (RCF). The well plate was placed in a Bio-Rad C1000 Thermal Cycler CFX96 Real-time system -device and the following program was set for qPCR: Step 1: 50°C for 2 min. Step 2: 95°C for 10 min. Step 3: 65°C for 30 seconds. Step 4: 72°C for 30 seconds and return to step 2 for 49 times. Step 5: 50°C for 30 seconds. Step 6: Melt curve from 65°C to 95°C with +0,5°C intervals every 5 seconds. For Myc qPCR, the temperature in steps 3 and 6 was 62°C.

4.7.1 qPCR for MYC gene

The forward primer MYC_F sequence was ACCAGAGTTTCATCTGCGACC and reverse primer MYC_R sequence was GGGTCGATGCACTCTGAGG. The calculated anneal temperature was 62°C and the expected product size 238 bp. The standard sample series for the MYC in the qPCR setup was a human cell line pool cDNA set for hi-MYC as a dilution series 1:5 (cDNA pool previously made).

4.7.2 qPCR for β-Actin-gene

The forward primer mBACTIN_ex4_F sequence was CGAGCGGTTCCGATGCCCTG and reverse primer mBACTIN_ex6_R sequence was ACGAGCTCAGTAACAGTCCGC. The calculated anneal temperature was 65°C and the expected product size 395 bp. The standard for the β-Actin in the qPCR setup was a mouse cDNA pool as a dilution series 1:5 (cDNA was pool previously made). β-Actin was used as a housekeeping gene since β-Actin is a very common protein in mammalian cells.

4.8 Normalization of hi-MYC expression with β-Actin expression data

Normalization was done with two methods to compare the results and to choose the most reliable one. The first method was a ratio of starting quantities ($SQ_{MYC}/SQ_{\beta\text{-actin}}$), in which the starting quantities were calculated based on the experiment. As the efficiencies were not the same for MYC and β-Actin, Pfaffl method (see formula below) was used as the second method.

$$Pfaffl\ ratio = \frac{E_{sample}^{\Delta Ct,sample(calibrator-test)}}{E_{reference}^{\Delta Ct,reference(calibrator-test)}}$$

Ct is that cycle's number in the PCR-reaction cycle, on which the fluorescence signal exceeds the chosen threshold. The threshold was kept at the level which was determined best by the Bio-Rad CFX-system; The threshold was in the linear area of the amplification curve. The calibrator was the standard pair 3 mean from the standard sample series.

4.9 Agarose gel electrophoresis

The gel for electrophoresis was made by mixing 0,6 g of molecular grade agarose (Bioline) and 60 ml of 0,5 x TBE-Buffer. The mixture was heated in a microwave oven with roughly 900 W power until the agarose had completely dissolved into the buffer. The liquid gel was cooled down and 6 µl of 10000 x Invitrogen SYBR Safe DNA Gel Stain was added. The liquid was poured down to a gel tray with a gel comb or two (depending on the number of samples). When the agarose gel had turned solid, the running buffer (TBE-buffer) was added to the tray so that the gel was submerged. Samples from qPCR were mixed each with 2 µl of 6x Loading dye (Thermo Fisher Scientific) and 10 µl of this sample mix was added to a well. When the agarose gel was cast with more densely packed gel combs, a smaller sample amount (8 µl) was used to avoid overflow from the wells. 5 µl of the GeneRuler 100bp (Thermo Fisher Scientific) was used as a ladder. The electrophoresis was carried out by applying 120 V and 400 mA electric current to the gel for 30 minutes. The result was imaged with UV light.

4.10 TaqMan assay

Previously synthesized cDNA was used in samples for TaqMan assay. The dilution ratio for each sample was 1:20. Standard sample series was made from cDNA extracted previously from 22Rv1 prostate cell line. The master mix was made for the qPCR by combining 54 µl of the TaqMan MicroRNA Assay 20x (miR-32-specific), 540 µl of the TaqMan Universal PCR Master Mix and 378 µl of nuclease-free water. 18 µl of the master mix was pipetted into wells of 4titude 96-well qPCR plate. 2 µl of the diluted cDNA/water/non-template-control/RT-control was pipetted into the wells. The well-plate was sealed and centrifuged for 1 min with 800 g. The TaqMan-assay was run in the Bio-Rad C1000 Thermal Cycler CFX96 Real-time system. The program for qPCR had 95°C temperature for 10 min as step 1, 95°C for 15 seconds as step 2 and 60°C for 1 min as step 3, after which fluorescence was measured. Program was set to repeat starting from step 2 altogether 39 times.

The data from detected FAM-type fluorescence in the assay was normalized to RNU6B, which is a common “housekeeping gene” and often used as a control gene (Remáková et al., 2013). The normalization of the miR-32 results was done by calculating a ratio of the mouse samples out of which miR-32-levels were assessed during the experimental stage, but out of which also RNU6B levels had been calculated previously.

4.11 Statistical analysis for IHC and qPCR experiments

Statistical analysis with IBM SPSS Statistics software version 23 was used on the results which required further analysis. For example, results from anti-PCNA-staining on dorsal, lateral and ventral

normal epithelium were analyzed because of the complicated nature of the data set: multiple groups had to be compared at the same time. 95% confidence interval was used as a criterium for statistical significance. The normality of distribution was assessed from all tested sample groups. The used statistical tests were ANOVA (one-way) and Student's t-test.

5. Results

5.1 Immunohistological analysis of mouse prostate

To analyze the presence of different marker proteins as a sign of activation of pathways they belong to, several model systems were used. The prostate samples were immunostained against different markers and the cells and nuclei containing them were analyzed in dorsal, lateral and ventral area of the prostate.

The next section presents some of the criteria used in the quantification. Examples are shown in the following images, which show typical views of the samples and the correct way of interpreting them. In the immunohistochemistry experiments, all quantification was performed by the thesis's author. Correct recognition of areas was confirmed by the thesis's supervisor.

5.1.1.1 Basic histology of mouse prostate

Shown in Figure 7, is an example view of the tissue from the dorsal, lateral and ventral lobes consisting of glandular structures. Dorsal lobe (7A) is characterized by scarce infolding of the epithelium to the lumen and with variable amount of secreted matter from eosinophils to the lumen. There may be stroma tissue surrounding the gland structure. The lateral lobe (7B) is located between dorsal and ventral lobes in the prostate and it usually has only a few infoldings of the epithelium. The ventral lobe (7C) usually has very little eosinophilic secretion to the lumen but has some tufting of the epithelium.

In each view in Figure 7, the areas where nuclei could be counted are also marked. As, for example, glands in the lateral lobe have relatively large lumen area and only a thin layer of cell in the epithelium, somewhat large areas had to be analyzed to fill the limit of 500 counted nuclei per sample area.

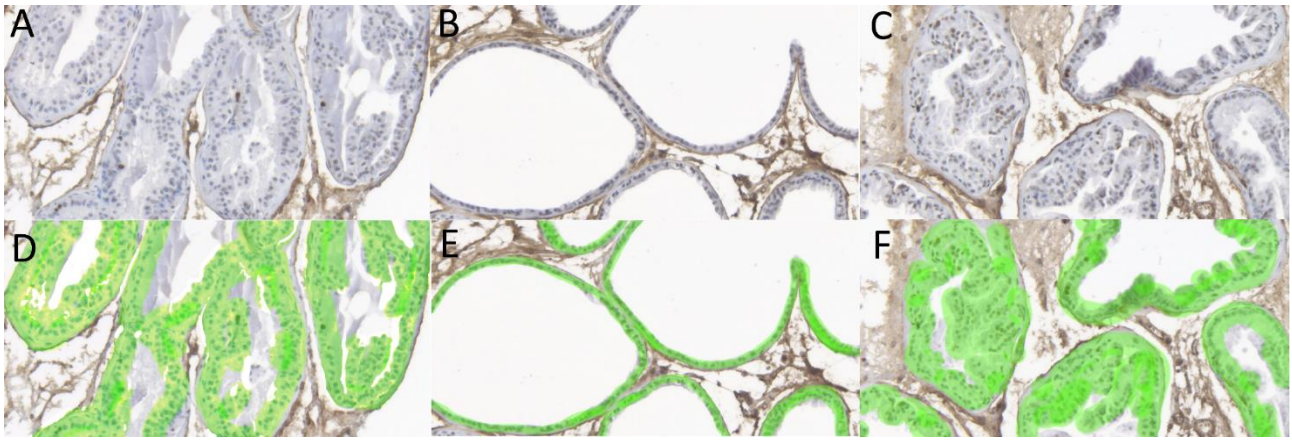

Figure 7. Examples of normal prostate epithelium in dorsal lobe (A), lateral lobe (B) and ventral lobe (C). The bottom of the panel (D-F) also shows in light green color the correct areas which could be used for nuclei

analysis for each lobe. Image is from normal epithelium analysis (miR-32 +/- genotype) with anti-PCNA-staining.

5.1.1.2 Mitotic marker P-H3

For analysis of mitotic rate, a primary antibody against mitotic marker P-H3 was used. The samples stained with P-H3-targeting antibodies were sorted in a binary fashion, i.e., either into the brown (positive) or the blue (negative) category. The Figure 8 below shows nuclei with brown stain and blue counterstain.

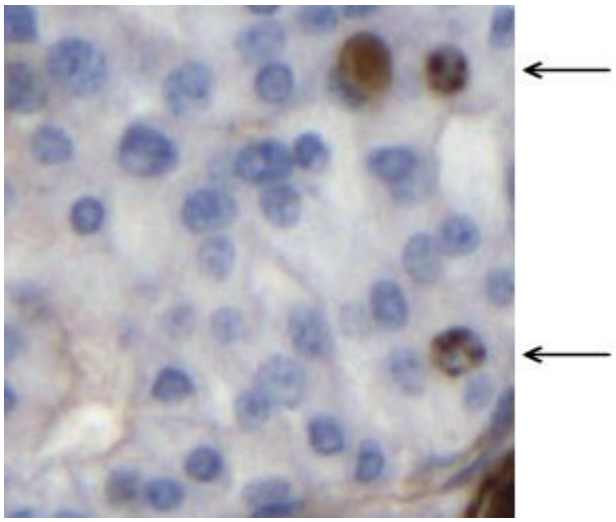

Figure 8. An example of staining with anti-P-H3-antibody. In this view, three brown stained P-H3-expressing nuclei can be seen and are pointed at with arrows. Image is from a neoplasia model sample (Pten+/- miR-32+/- mice) with anti-P-H3-staining.

5.1.1.3 Apoptosis marker cleaved caspase-3

To analyze rate of apoptosis in the tissue, the apoptotic marker cleaved caspase-3 was assessed. Samples which were stained with the cleaved caspase 3 -targeting antibody showed brown staining of nuclei and brown-stained apoptotic particles. Examples of stained nuclei and particles can be seen in Figure 9. The nuclei were sorted into category brown or category blue.

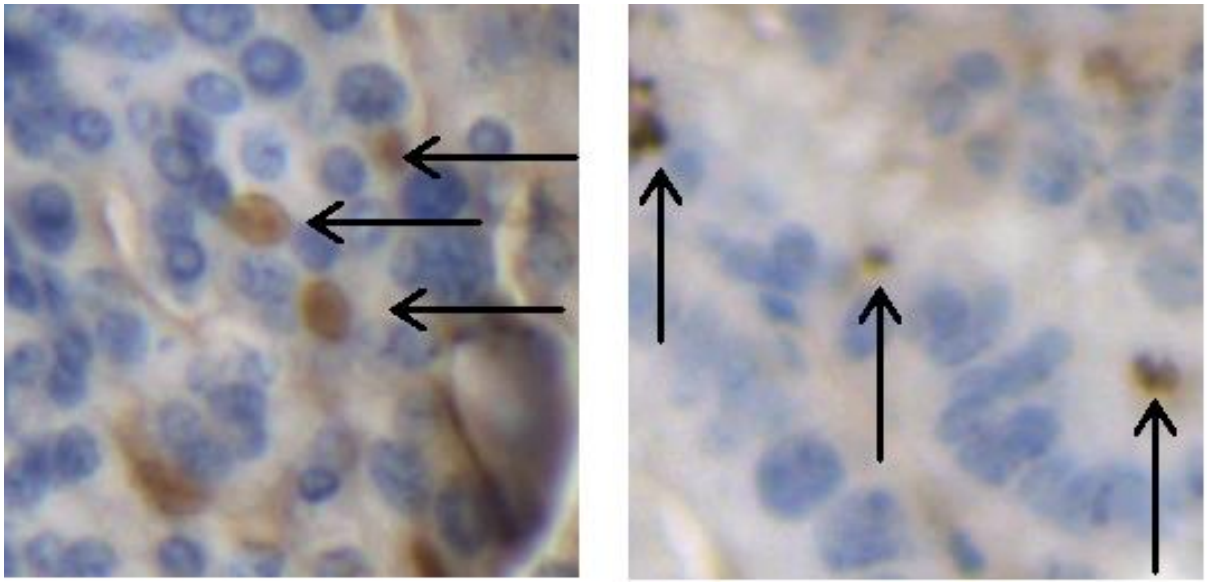

Figure 9. Example of staining with antibody targeting cleaved caspase 3. In the image on the left, whole nuclei stained brown are shown (arrows), whereas only stained apoptotic particles can be seen in the image on the right (arrows). Image is from a neoplasia model sample (Pten+/- miR-32+/- mice).

5.1.1.4 Proliferation marker PCNA

A system with HRP/DAB-chromogen and PCNA-targeting antibodies create a range of different shades of brown color depending on the amount of PCNA present in the nucleus. For quantifying the PCNA staining in the nuclei, four different categories were used: dark brown, medium brown, weak brown and blue. Nuclei from all these four categories can be found below in Figure 10.

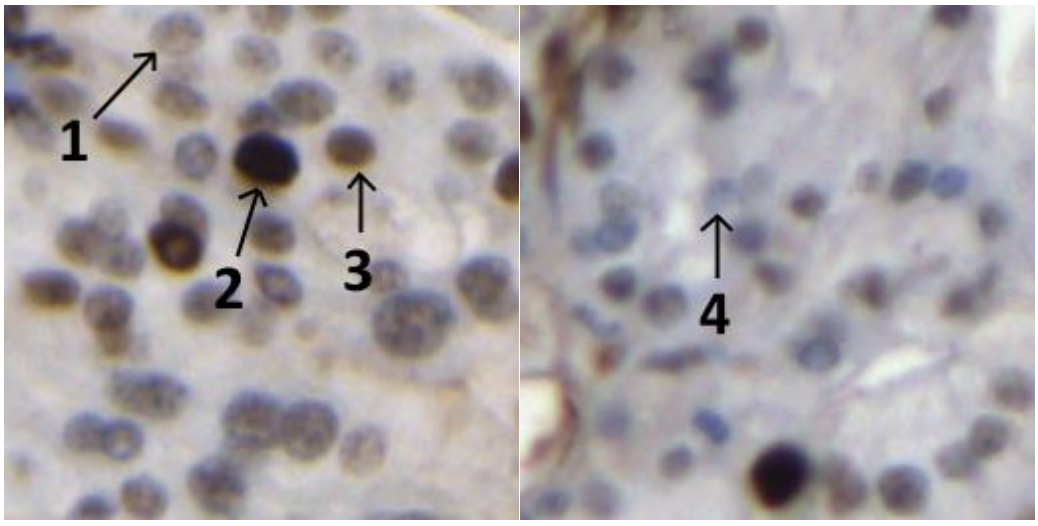

Figure 10. Example of different intensities of anti-PCNA-staining. The color gradient was divided into four classes. In the example pictures, number 1 stands for a weakly brown stained nucleus, 2 = dark brown, 3 = medium brown and 4 = blue. Image is from neoplasia model sample series (Pten+/- miR-32+/- mice).

5.1.1.5 PI3K/Akt/mTOR-pathway marker P-S6

Brown color produced by staining against P-S6 was not nuclei-specific, and manual counting could not be used and therefore ImmunoRatio-software was used instead. In Figure 11, the original image

and its pseudo-colored version by ImmunoRatio can be seen on the left side of the panel and the saturated image with its pseudo-colored version can be seen on the right side.

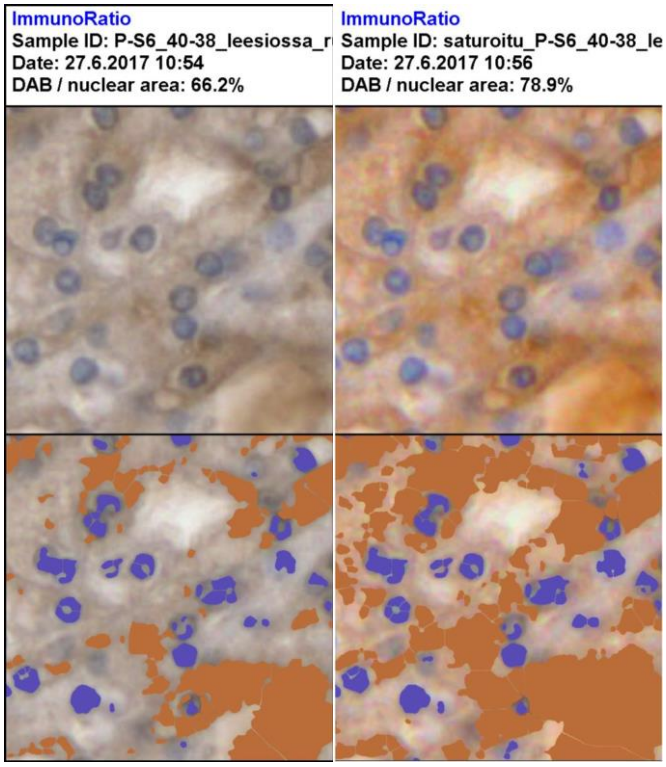

Figure 11. Comparison of the original and a saturated image in the ImmunoRatio-analysis. The original image (upper left) and the pseudo-colored image (bottom left) can be seen on the left side of the panel. The saturated version of the image with its pseudo-colored version can be seen on the right side. The computationally detected amount of brown stain was 66.2 percent and 78.9 percent in these cases, respectively. Image from neoplasia model sample series, mice genotype was Pten+/- miR-32+/-.

Analysis of a whole PIN-lesion from a sample of the neoplasia model series with anti-P-S6-staining can be seen in the image below (Figure 12). The upper image is the original saturated and cropped image and the one below is pseudo-colored.

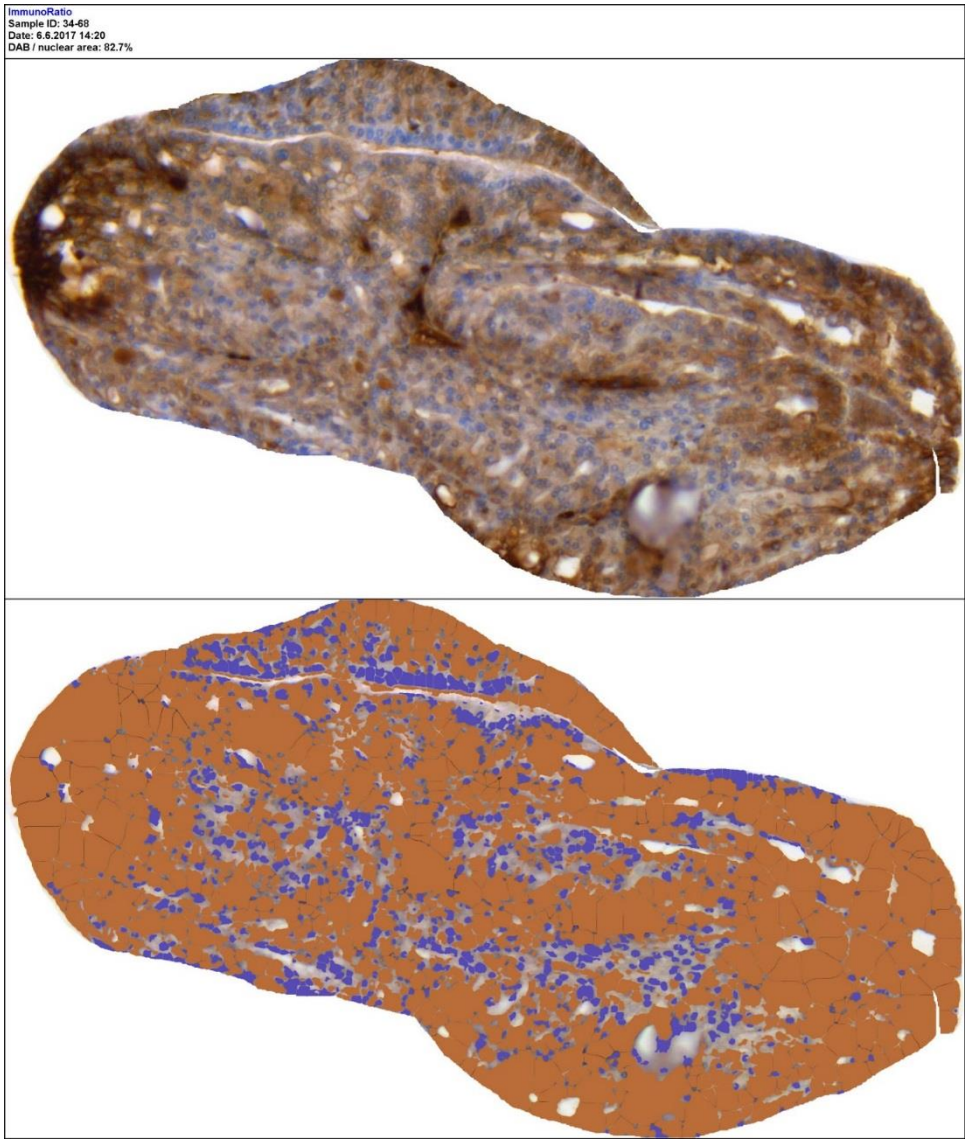

Figure 12. Immunoratio-analysis of a cropped and pre-saturated image of anti-P-S6-staining of a whole, high-grade PIN-lesion. The upper image is the original saturated and cropped image and the one below is pseudo-colored. The computationally detected amount of brown stain was 82.7% of the whole PIN lesion. The image is from the neoplasia model series (Pten+/- miR-32+/- mice).

5.2 Effect of miR-32 in normal epithelium

The normal epithelium was assessed in three different prostate lobes per sample: dorsal, lateral and ventral prostate area. These areas were stained with four different antibody markers to study the molecular processes in the normal state of the mouse prostate.

5.2.1 P-H3

Staining with anti-P-H3-antibodies produced partially abnormal staining. The last six slides in the set (out of 13) were probably inadequately rinsed and had had a too long staining time. The unrepresentative samples were excluded and the remaining data was used to produce the graph of the percentage brown nuclei in different tissue types, which is shown in Figure 13. The differences

between miR-32 positive and -negative sample group were not statistically significant in any prostate lobe.

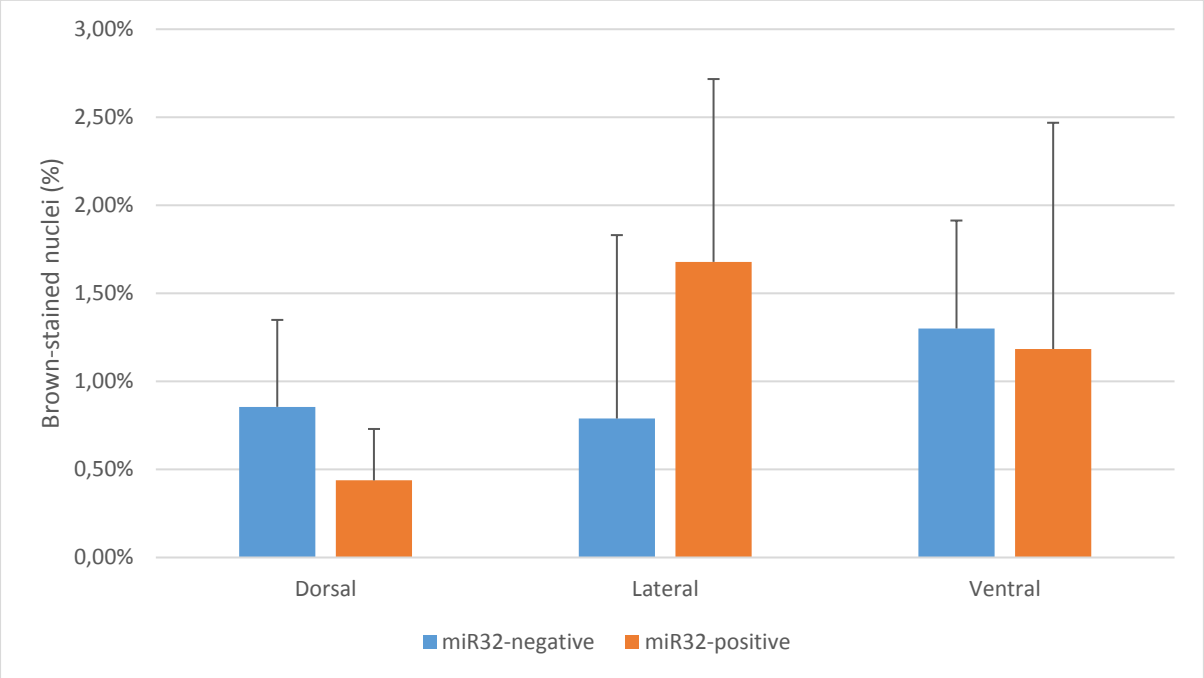

Figure 13. Percentage of brown nuclei in different lobes in normal prostate epithelium (miR-32 +/- genotype) with an anti-P-H3 -staining. ARR2PB-miR32-negative samples are shown in blue and miR32-positive in orange. Six samples out of 13 were excluded due to staining abnormality and are not shown here. Standard deviation (SD) is shown with bars. SD bars are shown only in only plus direction.

5.2.2 Cleaved caspase-3

The results of the staining against the cleaved caspase-3 in the normal epithelium samples were excluded, since the analysis result was likely affected by a bias.

5.2.3 PCNA

In the sample set with anti-PCNA-staining, there were four categories for staining and the same three prostate lobes as before. The anti-PCNA staining results are shown in all setups in Figure 14. The differences between ARR2PB-miR32-negative and positive sample groups were not statistically significant.

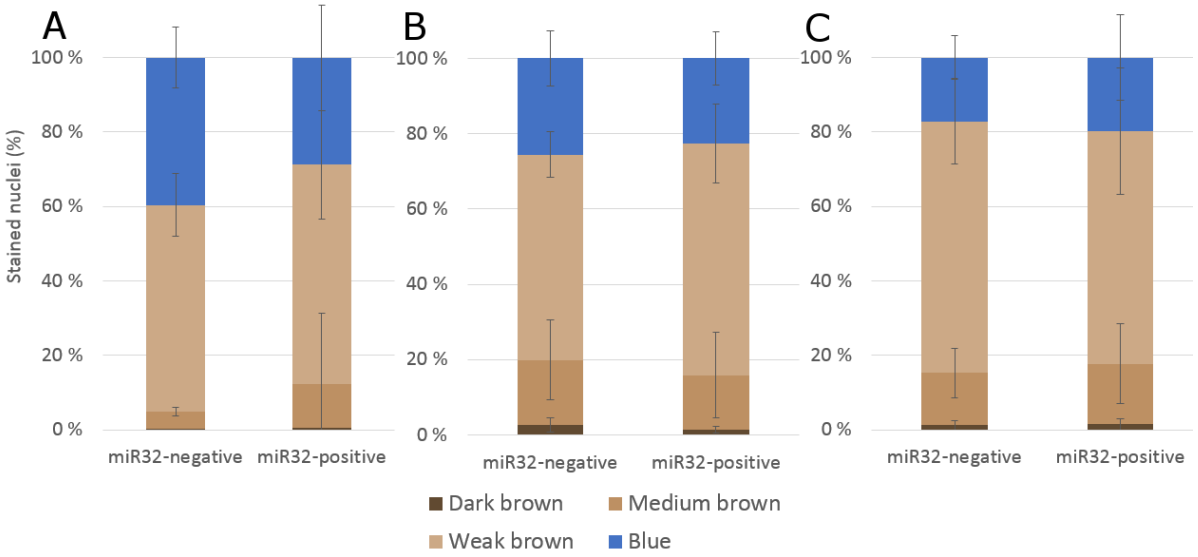

Figure 14. Combined graph from quantification of anti-PCNA-staining in normal epithelium (miR-32 +/-) in the three studied prostate lobes: dorsal (A), lateral (B) and ventral (C). Blue color represents the nuclei which were PCNA-negative and stained blue by the auxiliary stain. The shades of brown represent the PCNA-positive categories. Standard deviation is shown for each category. The MiR32-negative sample group is on the left side and the miR32-positive on the right side in the panels A, B and C.

Table 1 shows the results of the one-way analysis of variance for the PCNA-staining data. The results revealed no statistically significant differences (on 95% confidence interval) between the miR-32 positive and negative groups in any staining category in any studied prostate lobe.

Table 1. Comparison of miR-32 positive and -negative groups in anti-PCNA staining from normal epithelium with one-way-ANOVA. There is no significant difference (on 95% c.i.) between miR32-positive or negative samples in any prostate lobe (dorsal, lateral or ventral) in any staining category (dark brown, medium brown, weak brown or blue). Thus, possible differences between the compared groups are due to sampling error instead of a real biological phenomenon.

ANOVA

Location in prostate			Sum of Squares	df	Mean Square	F	Sig.
Dorsal	Percentage of dark brown stained nuclei	Between Groups	,000	1	,000	,311	,588
		Within Groups	,000	11	,000		
		Total	,000	12			
	Percentage of medium brown stained nuclei	Between Groups	,016	1	,016	,709	,418
		Within Groups	,254	11	,023		
		Total	,271	12			
	Percentage of weak brown stained nuclei	Between Groups	,004	1	,004	,225	,645
		Within Groups	,177	11	,016		
		Total	,181	12			
	Percentage of blue stained nuclei	Between Groups	,036	1	,036	2,400	,150
		Within Groups	,167	11	,015		

		Total	,203	12			
Lateral	Percentage of dark brown stained nuclei	Between Groups	,000	1	,000	2,969	,113
		Within Groups	,002	11	,000		
		Total	,002	12			
	Percentage of medium brown stained nuclei	Between Groups	,002	1	,002	,184	,676
		Within Groups	,134	11	,012		
		Total	,136	12			
	Percentage of weak brown stained nuclei	Between Groups	,015	1	,015	1,745	,213
		Within Groups	,092	11	,008		
		Total	,106	12			
	Percentage of blue stained nuclei	Between Groups	,003	1	,003	,503	,493
		Within Groups	,057	11	,005		
		Total	,059	12			
Ventral	Percentage of dark brown stained nuclei	Between Groups	,000	1	,000	,099	,759
		Within Groups	,002	11	,000		
		Total	,002	12			
	Percentage of medium brown stained nuclei	Between Groups	,001	1	,001	,168	,690
		Within Groups	,097	11	,009		
		Total	,099	12			
	Percentage of weak brown stained nuclei	Between Groups	,008	1	,008	,343	,570
		Within Groups	,256	11	,023		
		Total	,264	12			
	Percentage of blue stained nuclei	Between Groups	,002	1	,002	,222	,647
		Within Groups	,106	11	,010		
		Total	,108	12			

5.2.4 P-S6

The normal epithelium analysis from anti-P-S6-stained cells was performed on dorsal, lateral and ventral prostate areas. Staining was analyzed on IIPImage viewer (http://iipimage.sourceforge.net/) on a semiquantitative scale, where the categories of either <10%, 10%-50%, or >50% positive (= brown) tumor cells were used. The method was originally used by Vicente et al. (2017). The method is only semiquantitative (like almost all IHC-related methods), so the results should be interpreted with certain reservations.

The results were also dichotomized into P-S6 positivity and negativity for simpler data interpretation. In the dorsal lobe, 75% of miR-32 positive samples were expressing P-S6 whereas a slightly smaller proportion (60%) of miR32-negative samples were P-S6 positive. In the lateral lobe, only 50% of miR32-positive samples expressed P-S6 compared to the higher amount of 80% in

miR32-negative samples. The ventral lobe showed almost the same expression level of P-S6 in miR-32 positive or negative samples: 62.5% and 60%, respectively.

5.3 Effect of miR-32 in intraepithelial neoplasia

In the PTEN-heterozygote neoplasia model mice group, the assessed area was the high-grade PIN lesions of mice with a germline deletion of one allele of the PTEN gene. One group of the mice were ARR2PB-miR32 positive and the other ARR2PB-miR32 negative. The results in this section represent the intraepithelial neoplasia -like mouse prostate state.

5.3.1 P-H3

When staining with anti-P-H3-antibodies and miR-32-negative mice samples, 2.92% of counted nuclei were stained brown whereas the majority were blue with a 97.55% share. Only a fraction of more brown nuclei was found in miR-32-positive mice samples; 3.18% of nuclei were stained brown and 97.78% stained blue. The results are shown as a graph in Figure 15.

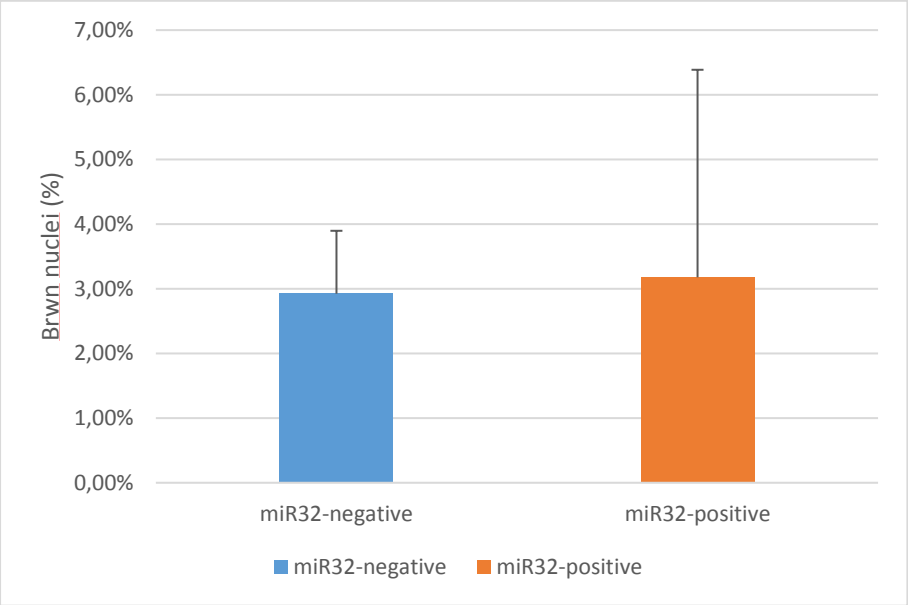

Figure 15. Average percentages of brown stained nuclei in high-grade PIN-lesions (Pten+/- miR-32+/- mice) in a staining with anti-P-H3 -antibodies. The miR-32-negative group is shown in blue and the positive in orange. Standard deviation (SD) is shown with bars. SD bars are shown only in only plus direction

5.3.2 Cleaved caspase-3

In the staining with antibodies targeting cleaved caspase-3-antibodies in miR-32-negative mice samples, only 1.51% of counted nuclei were stained brown and 98.59% blue. In the miR-32-positive sample group, only 1.41% of nuclei were stained brown and the remaining 98,59 % stained blue. The results are shown in Figure 16 as well.

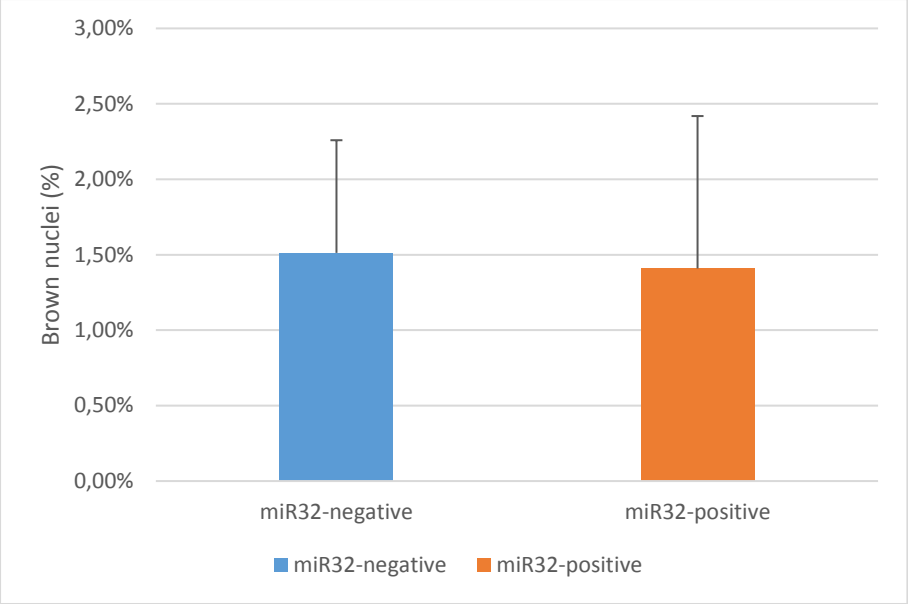

Figure 16. Average percentages of brown stained nuclei in high-grade PIN-lesions (Pten+/- miR-32+/- mice) in a staining with anti-cleaved caspase-3 -antibodies. The miR32-negative group is shown in blue and the positive in orange. Standard deviation is shown with bars.

5.3.3 PCNA

The results for the anti-PCNA-staining of the PIN lesions are presented in Figure 17. The t-test on independent samples (not shown) confirms that there are no statistically significant differences between the miR32-positive and -negative sample groups.

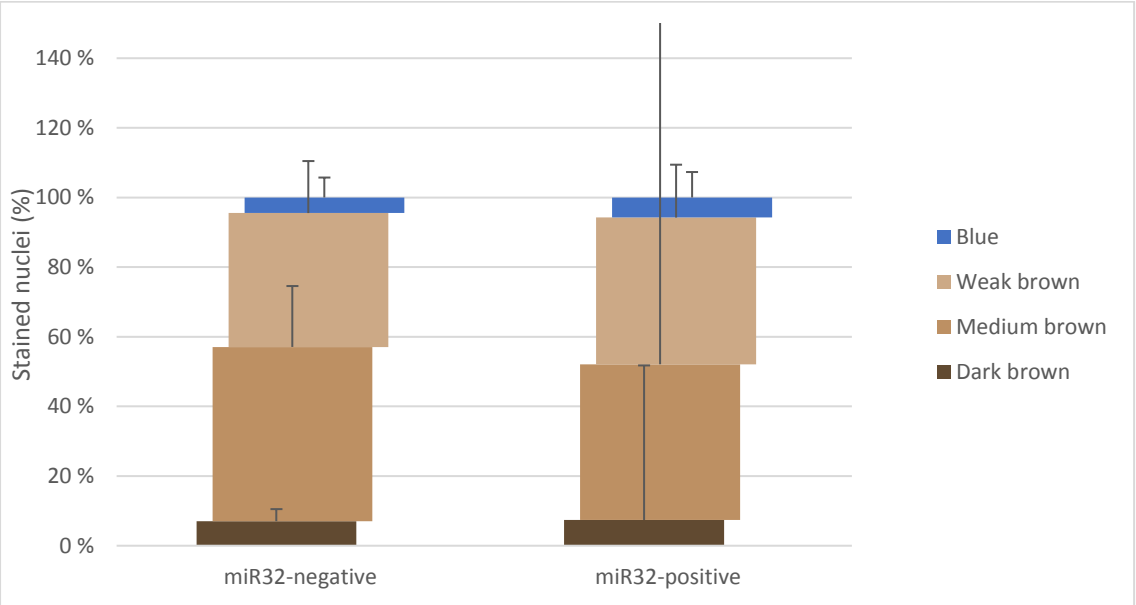

Figure 17. Average percentages of brown stained nuclei in a staining with anti-PCNA antibodies, mouse genotype Pten +/- miR-32+/-. The miR32-negative group is on the left and the positive on the right side. Chart groups are tilted to enable analysis of the otherwise overlapping standard deviation (SD) bars..

5.3.4 P-S6

Figure 18 shows the amount of brown stain in the high-grade PIN lesion. The staining was quantified with the Immunoratio-software (jvsmicroscope.uta.fi/immunoratio/). The amount of brown varies between 47 and 92 percent and the average values for the ARR2PB-miR32 -negative and -positive samples are 84.1% and 73.1%, respectively. The two groups have 12.4 percentage units of difference in means, which is not statistically significant on 95% confidence interval, since standard error is 7,27 and p = 0,12.

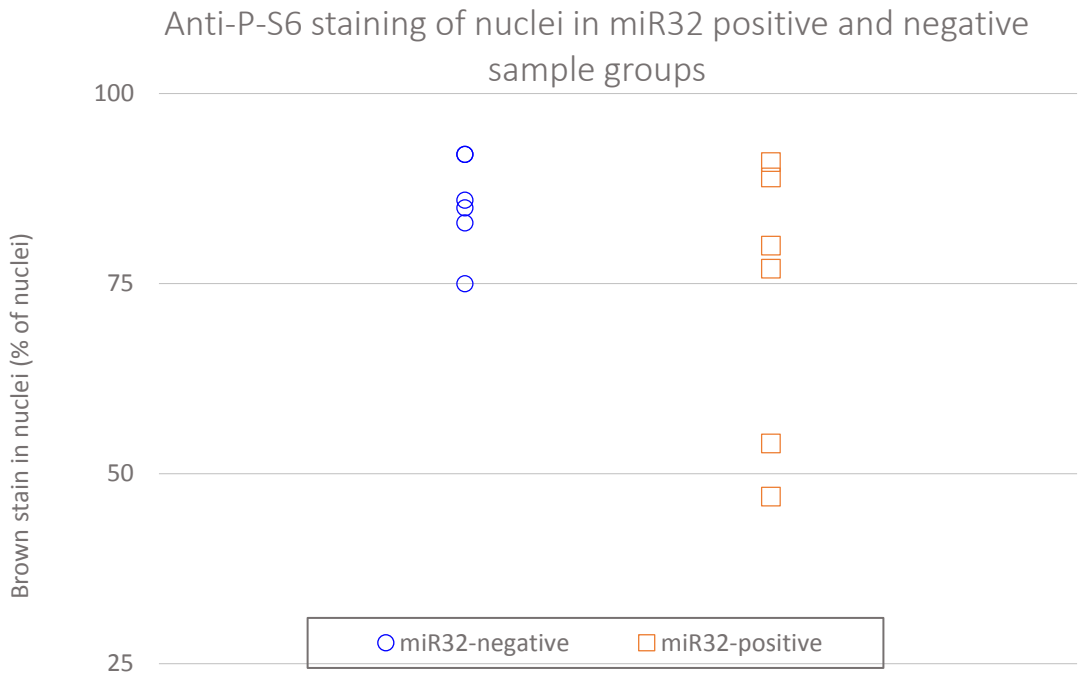

Figure 18. Percentage of the brown area in lesions in samples in Pten+/- miR-32+/- mice with anti-P-S6-staining. The ARR2PB-miR32-negative samples are shown as hollow blue circles and the positive as hollow orange rectangles. Difference between the two groups is not statistically significant.

5.4 Effect of miR-32 in primary prostate cancer model

In this series, the results were gathered by analyzing the lateral area and the tissue type was meant to represent the primary prostate cancer -like state of the mouse prostate, which expresses Myc gene on a high level. The glands of the lateral lobe were either visibly stained and grown-in or normal-looking. The obvious difference between these two could pose a problem for the blinding assumption (see Discussion).

The series with anti-Ki-67 and anti-cleaved caspase 3 -antibodies were done with a different immunohistochemistry protocol than the anti-P-H3-staining. The results for P-H3, cleaved caspase-3 and Ki-67 are shown in Figure 19, Figure 20 and Figure 21, respectively.

5.4.1 P-H3

The antigen retrieval buffer used here was pH 9 Tris-EDTA buffer, thus this sample set is different than the cleaved caspase 3 and Ki-67-stainings. In the results (Figure 19), two groups can be distinguished: those with brown nuclei amount close to zero and those with over 5% of brown nuclei out of total. To simplify, the samples which had active Myc expression had brown stained nuclei and those which were Myc-negative, were also P-H3 negative. MiR-32 expression did not seem to have an effect.

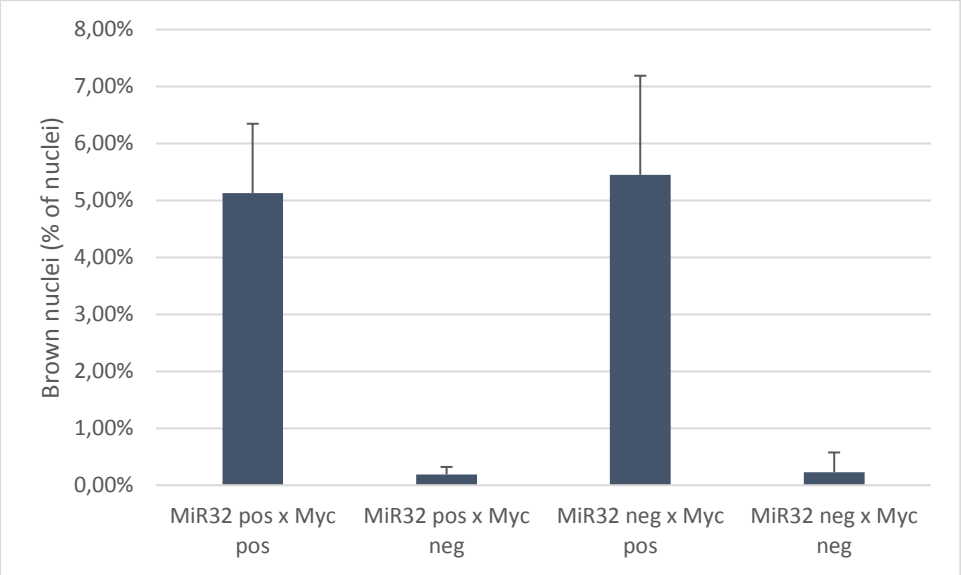

Figure 19. Analysis of P-H3-stained nuclei in samples from mouse with miR-32 +/- Myc +/- genotype. The four genotypes are shown in the x-axis. Standard deviation is also shown.

5.4.2 Cleaved caspase-3

The antigen retrieval buffer used here was the sub-optimal pH 6 citrate buffer. The staining was weak partly because of this. As a result, almost all the counted nuclei were blue and there are no large differences between the four genotypes (Figure 20).

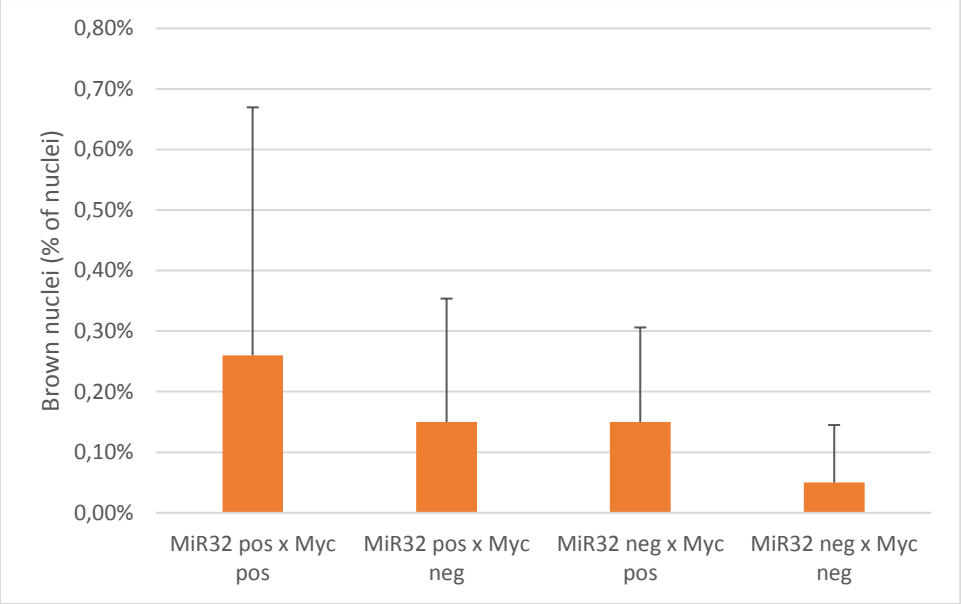

Figure 20. Analysis of nuclei stained against cleaved caspase-3 in in samples from mouse with miR-32 +/- Myc +/- genotype. The four genotypes are shown in the x-axis. Standard deviation is also shown (bars).

5.4.3 PCNA

The staining outcome was too weak for observations, and therefore this sample set was not scanned nor analyzed.

5.4.4 Ki-67

Two groups of samples can be distinguished in the results (see Figure 21). Ki-67-expression was relatively strong (~15% of positive nuclei) in the samples which had hiMyc-expression and respectively, the brown staining by Ki-67 was almost absent if the sample group was Myc-negative. MiR-32-expression did not seem to have any effect. The antigen retrieval buffer used here was the sub-optimal pH 6 citrate buffer.

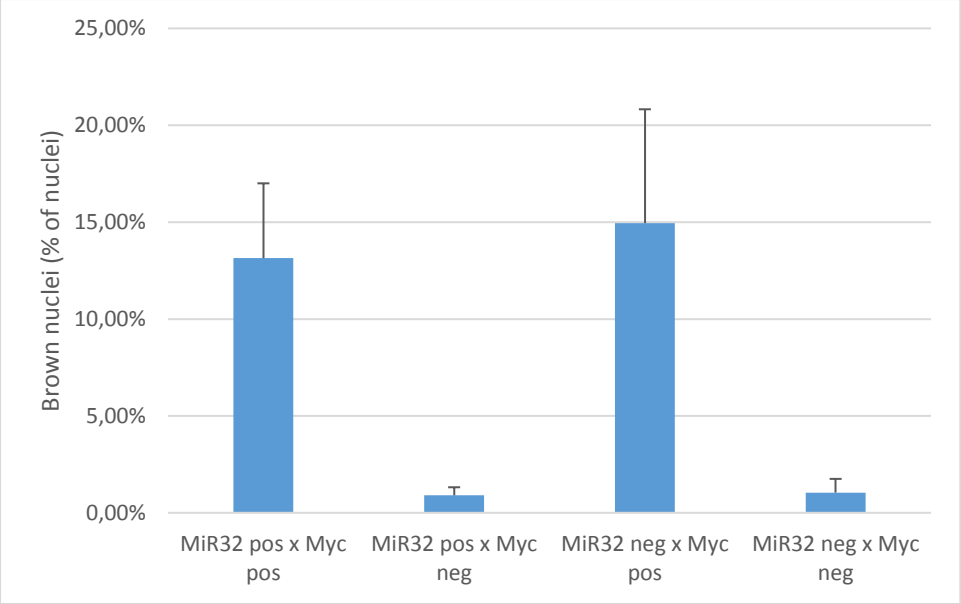

Figure 21. Analysis of Ki-67-stained nuclei in samples from mouse with miR-32 +/- Myc +/- genotype series. The four genotypes are shown in the x-axis. Standard deviation is also shown.

The quantification was done partly with the Immunoratio software. The results (not shown here) were systematically different – usually a lower percentage of positive nuclei – from the results obtained by calculating manually, so the Immunoratio-results for Ki-67 were omitted. The Immunoratio method also required image manipulation for each sample, but the time used per image was on average roughly a minute shorter than the time required for manual counting.

5.5 Analysis of expression of transgenic MYC

As well as the samples used for immunohistochemistry, the samples used here represent a primary prostate cancer model in this study. The samples were stored frozen before use.

The successful RNA extraction was confirmed each time by absorbance measurements with Nanodrop 2000 device. The results, i.e., the absorbance measurements and ratios from them are presented in the supplementary Table 4. The absorbance ratio of wavelengths 260 nm / 280 nm provides an estimate of the purity of the nucleic acid, in this case the RNA. The ratio is acceptable for each sample, even though there was some variation between the lowest and the highest value: 2,06 and 2,49.

Assessing the absorbance ratio 260/230 helps to identify possible contaminants; the obtained 260/230 ratios were poor and variable between the different samples. A contaminant is therefore suspected. The purity could have been enhanced had it been necessary (see Discussion). The concentration values, which were calculated from absorbance measurements, are also shown in

Table 4. The concentration in the sample set was very variable, ranging from 30 ng/µl to over 360 ng/µl.

The cDNA synthesis process, which was done using the extracted RNA, was not quantified itself, but the successful synthesis was confirmed by successful qPCR with the SYBR Green and the TaqMan techniques.

Quantitative PCR was performed to find out, if Myc is expressed with ARR2PB construct in the used samples. The qPCR with the SYBR Green technique was successful in amplifying the Myc DNA, which confirms the presence of Myc gene transcripts in the samples.

Based on the linear standard curve, an efficiency of 116.8% was calculated and a R^2 value of 0,971 was obtained. The R^2 -value was below the optimal area (>0,98), and the efficiency value (116.8%) was also not in the optimal zone (95–105%) but still acceptable. β-Actin's standard curve from the qPCR gave a R^2-value (0,997) which is nearly optimal, while the calculated efficiency (92.5%) was near but not quite optimal. In addition to the linear standard curve, melt peak graphs were also formed. The melt peak graphs for both Myc-qPCR and β-Actin-qPCR-run had two distinct peaks (see Discussion).

The data from the qPCR measurements of the test gene Myc and the housekeeping gene β-Actin were compared to create a normalized data set for the Myc gene. The normalization was calculated by two methods. The calculation results of normalized value for each sample with Pfaffl method and SQ ratio is shown in Table 5, and the comparison of the results of both methods is shown as a graph in the Figure 22.

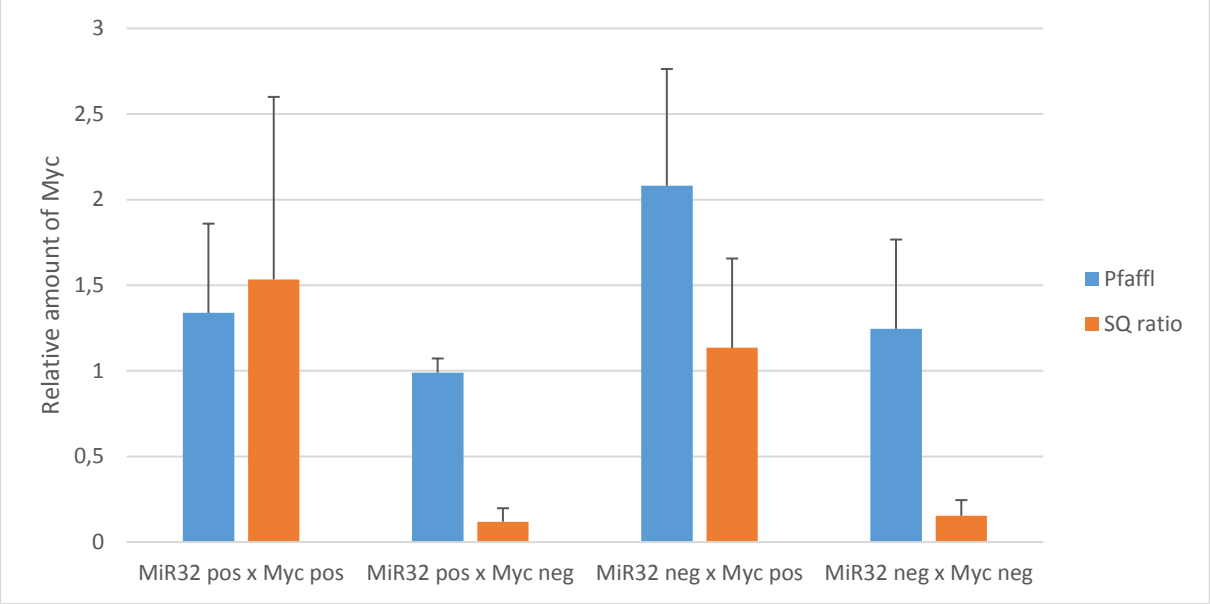

Figure 22. Comparison of the Pfaffl method (blue bars) and the SQ ratio (orange bars) in determining best method for MYC gene qPCR data normalization from samples with miR-32 +/- Myc +/- genotype. SQ ratio shows the highest relative amount in sample groups which are Myc-positive by genotype, whereas the Pfaffl method produces data with overlapping standard deviation. Pfaffl method data can be ambivalently interpreted, which could pose a problem.

The results of the qPCR assay for Myc and β-Actin were confirmed with agarose gel electrophoresis (AGE). An example of the results from AGE for Myc samples is shown in the Figure 23.

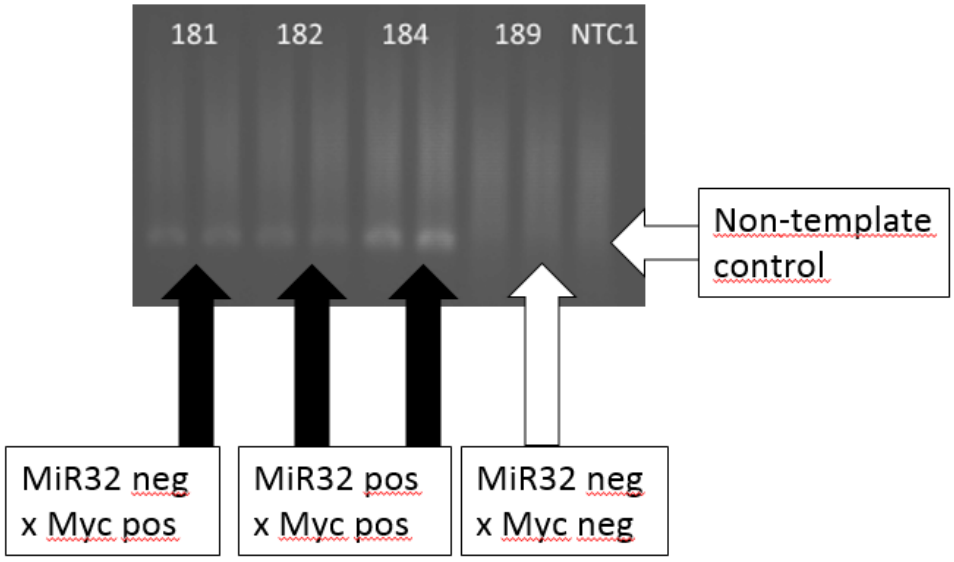

Figure 23. An example image of agarose gel after electrophoresis with Myc gene samples from qPCR (miR-32 +/- Myc +/- genotype). A band is seen in the samples which were Myc-positive by genotype (181, 182 and 184) but not in Myc-negative or control samples. The samples are numbered and the NTC1 is a non-template control. Image obtained from GeneSnap with UV light, exposure time 80 ms. Image adjusted for brightness (+100 units) and contrast (+50 units) in paint.net -software. All tested samples are not shown.

As expected, Myc-DNA-bands could be seen in the samples where the genotype was Myc-positive. These Myc-positive samples were simultaneously also either miR-32-positive or miR-32 negative. Accordingly, no band was noticeable in Myc-negative samples or in non-template controls.

AGE results confirm the presence of β-Actin in all qPCR samples disregarding non-template controls and the most diluted standard series samples. The results of electrophoresis with β-Actin samples are shown in Figure 24.

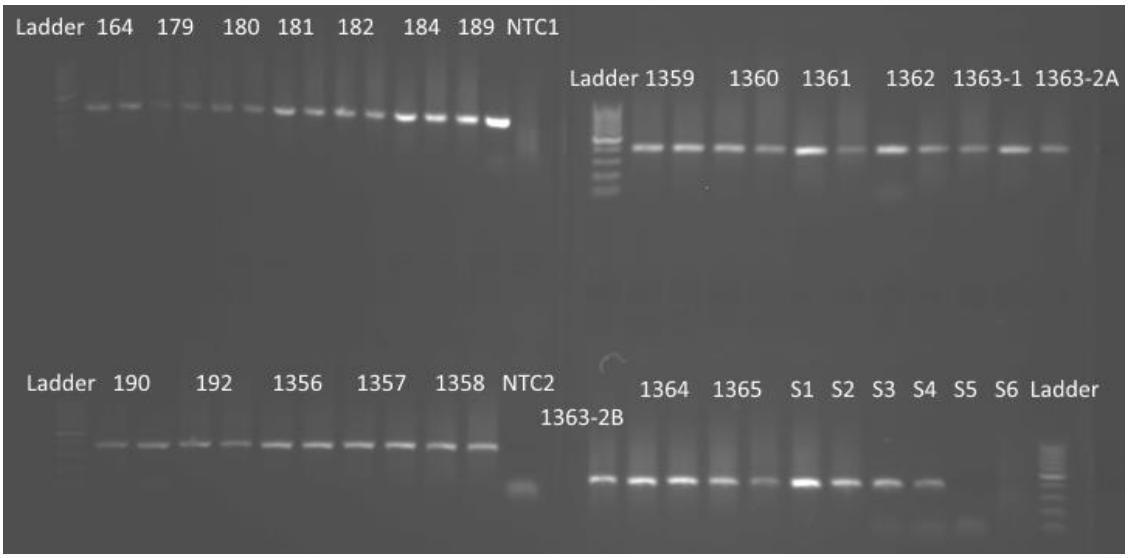

Figure 24. An image of agarose gel after electrophoresis with housekeeping gene β-Actin samples from qPCR, samples with miR-32 +/- Myc +/- genotype. Visible bands of β-Actin-DNA can be seen in all samples except in the controls (NTC1 and 2) and the most diluted standard samples (S5 and S6). Samples are numbered; NTC = non-template control and S1, S2, etc. are the standard sample series. Image taken with GeneSnap and with UV light, exposure time 80 ms. Image adjusted for brightness (+100 units) and contrast (+50 units) in paint.net - software.

5.6 Analysis of transgenic miR-32 expression

TaqMan assay was performed to confirm the presence of miR-32 in the used samples. The genotyping confirmed, that miR-32 was still actively expressed in samples, which were miR-32-positive by genotype.

Some of the samples did not reach high enough amplification levels to get a Ct value. The value for these samples was manually changed as 0,1 to represent a value close to zero to enable calculations for data normalization. All the amplification curves were cut out because the program had only 39 repeat cycles, but this did not prevent using the data. Efficiency was declared acceptable (E = 151.9%) and the R^2 value (0,995) was above the advised threshold (>0,980).

The miR-32 data was normalized to RNU6B housekeeping gene. Figure 25 shows the grouped normalized values, which were obtained as a ratio of calculated starting quantities.

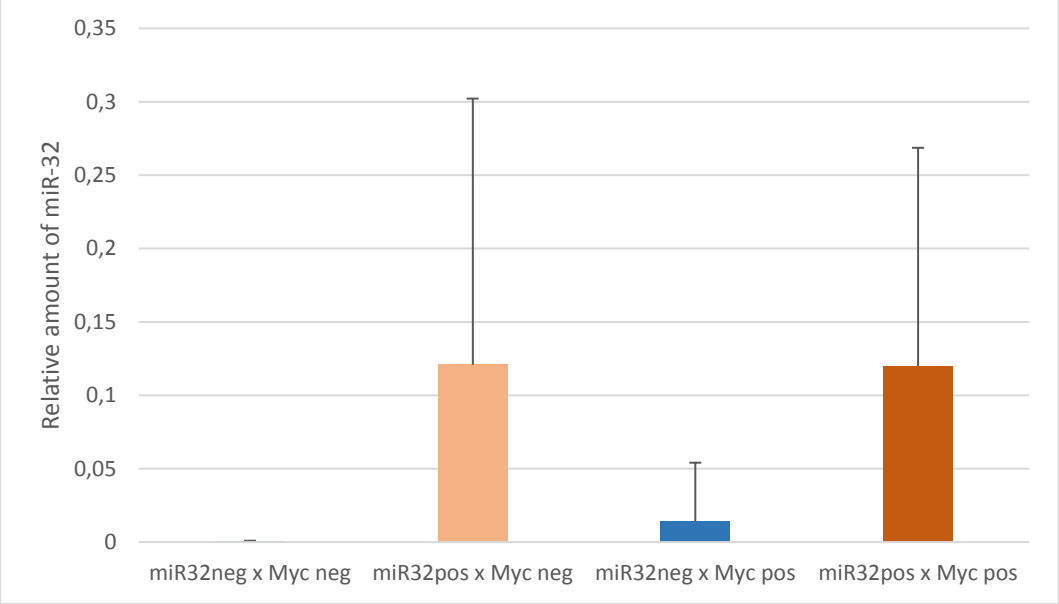

Figure 25. Ratio of calculated starting quantities of sample gene miR32 and reference gene RNU6B (small nucleolar RNA, snoRNA). Samples have four different genotypes: miR32 negative x Myc negative (1st group), miR32 positive x Myc negative (2nd group, light orange), miR32 negative x Myc positive (3rd group, blue), miR32 positive x Myc positive (4th group, orange). The standard deviation in positive direction is shown in the graph.

6. Discussion

6.1 Analysis of effect of miR-32 in normal prostate epithelium

The normal mouse prostate (i.e., without induction of cancer-like states) was assessed on the dorsal, lateral and ventral lobe areas. The study of normal epithelium in the three lobes of prostate in mice with either miR-32-positive or -negative samples aged 3-6 months demonstrated that the differences between the two genotypes were quite scarce.

The experiments with the normal mouse prostate and cleaved caspase 3-staining possibly had a bias, and the data is therefore not represented. Assessment seemed to produce more and more apoptosis-positive nuclei towards the last analyzed samples. Differences in apoptotic cell amount in normal epithelium between miR-32-positive and -negative sample groups can be caused by this bias. If stricter criteria would have been used, the outcome could have possibly been more consistent.

Also, some of the data from anti-P-H3-stainings had to be excluded. The rest of the data was used to evaluate presence of mitosis in the cells in the normal epithelium. The data had somewhat large variation and did not reveal statistically significant effects in any lobe.

The other two markers which were stained against were the nuclear proliferation marker PCNA and the cellular marker P-S6. The data from evaluation of the staining experiments with the PCNA would suggest that there was no statistically significant difference (at 95% confidence interval) in proliferation between the miR-32-negative and -positive sample groups in any lobe (dorsal, lateral or ventral) in any staining category. The P-S6 expression was detected in 50–80% of the samples depending of the group, but P-S6 was not consistently expressed more in either miR-32-negative- or miR-32-positive group. This most likely means that PI3K/Akt/mTOR-pathway was as active in both cases.

The relatively normal state of the mouse prostate would therefore consist of low mitosis activity and of relatively high proliferation and apoptosis activity, in addition to the relatively active PI3K/Akt/mTOR-pathway. Minor differences between miR-32-positive and negative sample groups may be lobe-specific or just arise out of the experimental setting.

6.2 Analysis of miR32 effect with a neoplasia model

The mice with Pten+/- genotype served as a model system for neoplasia- and intraepithelial neoplasia conditions in mouse prostate. To create the phenotype, the mice had a genotype, where one allele had been removed from the PTEN gene to induce high-grade PIN-lesions but also a miR-

32-expressing transgene had been inserted. The transgene was activated three generations ago. The two traits had been combined by crossbreeding the mice strains.

The immunohistochemistry experiments were not able to point out differences between miR-32-positive and -negative groups within the high-grade PIN-lesions of the PTEN-heterozygous mouse model in this age group, in which the mice were 10–11 months old.

In the tested samples, the PCNA protein and phosphorylated S6 protein were prominent, so it can be concluded that the cells in the PIN-lesions were actively proliferating and quite likely had active S6-kinase, which would suggest activity in PI3K/Akt/mTOR-pathway, which is linked to the cell cycle (see Figure 2).

The mouse model had lesser PTEN-expression due to removal of one allele, so it is expected that PI3K/Akt/mTOR-pathway was active in absence of inhibition from the PTEN, which is a phosphatase antagonizing PI3K (Di Cristofano et al., 1998; Song, Salmena, & Pandolfi, 2012; Wise et al., 2017). Particularly, the PI3K/Akt/mTOR-pathway activation leads to activation of proteins such as Myc to boost protein synthesis. The pathway also regulates the cell proliferation and metabolism via several proteins (Song et al., 2012).

Based on the PTEN/miR-32 immunohistochemistry experiments data, it would seem that the level of apoptosis was low in the studied PIN-lesions. Yet, one caspase alone may not be sufficient to confirm the apoptosis status of a studied mouse tissue, so using multiple apoptosis markers would have been ideal (Kaushal, Herzog, Haun, & Kaushal, 2014).

As the PTEN-model was intended to represent conditions of prostatic neoplasia – especially PIN-lesion - in the study, it could be said that a slowly developing benign tumor cell population would therefore have low mitosis and apoptosis activity and have quite an active proliferation pathway and PI3K/Akt/mTOR-pathway. It could also be said that the conditions in the neoplasia-modeling mouse prostate epithelium were quite similar with the normal mouse prostate epithelium, even though these two were not of same age and experimental settings were slightly variable. Another interpretation of results would be that miR-32 probably does not have a major role in neoplasia formation.

Primary prostate cancer model with miR32The samples with the MiR-32/Myc-genotype represented a model of a primary prostate cancer in this study. In the analyzed lateral prostate area, major differences between the miR32-positive and -negative groups were not found. The Myc-positive mice were from 3 months old age group.

An un-optimal antigen epitope retrieval buffer was used during the staining for three out of four sample sets. Because of this, the quality of the staining is not optimal these cases. The anti-PCNA-stained slides were not analyzed because the staining was too weak for evaluation. However, in the anti-Ki-67 and -cleaved caspase-3 staining, the staining outcome was not optimal, but still valid for assessment. Therefore, results of Ki-67- and cleaved caspase -3 analysis should be only compared to each other and not to the anti-P-H3-staining. This is, because the P-H3-staining was done with a more suitable epitope retrieval buffer, which had pH 9 instead of pH 6. The analysis was carried out by counting the brown and the blue nuclei.

The immunohistochemistry experiments with Ki-67 and P-H3 as markers showed quite clearly that samples with Myc-positive genotypes had highest expression: in the anti-Ki-67-staining there were about 13–15% of positive nuclei, and in anti-P-H3-staining over 5%. On the contrary, the miR-32-positivity or -negativity in the genotype did not seem to have an effect. Cleaved caspase-3-stained samples had a very low expression level, and therefore the miR-32-positive and -negative groups can't be compared to the positive group because of the very low expression level in the first place.

The data would suggest, that as well as in the normal epithelium and in the neoplasia model, only a small amount of the studied cells in the Myc-series' samples had the mitosis-specific phosphorylation pattern in the tail region of the histone 3's. This is somewhat surprising, as the conclusion would be that in a semi-advanced prostate cancer model (hiMyc-expressing mice), the replication and mitosis level would have been quite low (~5%), whereas the proliferation level would have been a bit higher (~15%) at the same time. However, the proliferation level was much lower than the percentages obtained from normal epithelium and PTEN-series samples epithelium analysis with PCNA as a proliferation marker. This may be, because the phosphorylation of the histone 3 is detected mainly only during the short mitosis phase (Pérez-Cadahía, Drobic & Davie, 2009), whereas for example, the proliferation marker Ki-67 may be present at any stage except quiescent phase (G_0) Scholzen & Gerdes, 2000). Ki-67 is often used as a proliferation marker, even though its function is not well known (Scholzen & Gerdes, 2000).

The conclusion of the staining experiment with Myc+/- miR32+/- samples could be formulated so that the active Myc expression in the mouse prostate contributed to the active Ki-67 expression, which is expected as both are closely related to cell proliferation. If PCNA-data had been available, the active proliferation could have been proven with more certainty. Myc expression may have had an effect on mitosis, based on the level of the detected P-H3. MiR-32-positivity or negativity in the genotype did not seem to have significant differences in the in primary prostate cancer -like conditions.

6.2.1 Quantifying images of IHC-stained slides

Three different series of samples were used for immunostaining experiments, and there were some inconsistencies in results inside the series and slightly different methods between the series. These cases are discussed in the next sections.

6.2.1.1 Normal epithelium

In the normal epithelium analysis, the quantification of immunostaining had some flaws. In the study of normal epithelium, too many nuclei were accepted as cleaved caspase 3 -positive. A trend could be seen, where the samples analyzed last were quantified to have more and more of brown staining. This means that the criteria should have been stricter (to accept only nuclei with granular brown particles or apoptotic particles) and it should have stayed unchanged during the quantification process.

The analysis of normal epithelium with staining against P-H3 was also hindered by abnormal staining of six samples (out of 13). The panel below (Figure 26) shows examples of varying staining outcomes with images from two sample slides. One group of the stained slides was very intensely stained and the other was not, which made it difficult to quantify the tissue. The too strongly stained group was excluded from the data shown in results.

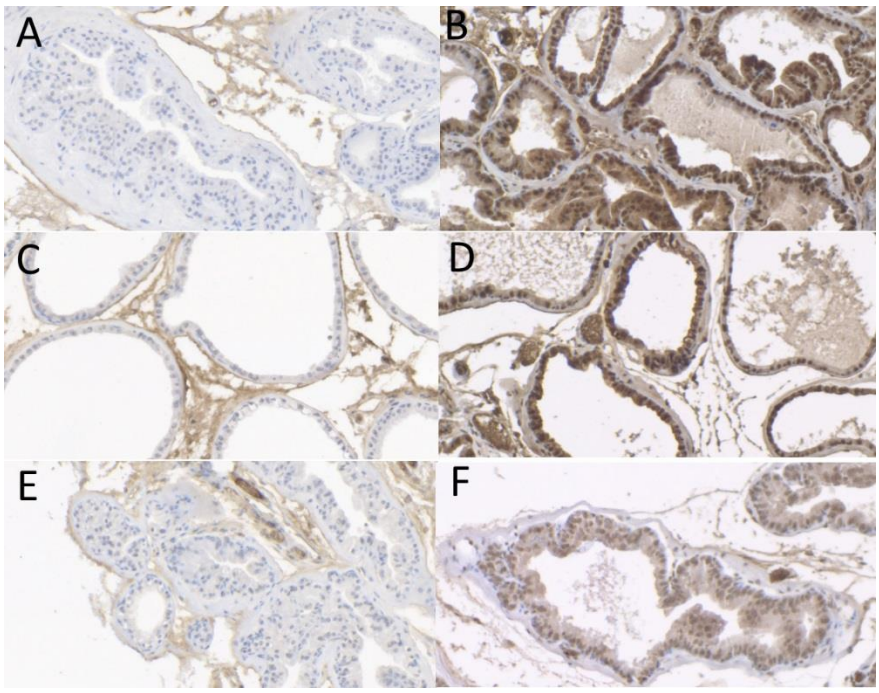

Figure 26. Abnormal staining in the anti-P-H3 staining of normal epithelium (mir-32 +/-): The staining was either very intense (B, D and F) or almost absent (A, C and E). The examples are from mice number 366 (left side) and 401 (right side). A–B=dorsal tissue, C–D=lateral tissue, E–F=ventral tissue.

For the analysis of P-S6-stained normal epithelium samples, different methods were compared. Some methods had quantitation of both the number of stained cells and the intensity of the stain

(Chaisuparat et al., 2016; Iwenofu et al., 2008), some preferred only evaluation of intensity (Egervari et al., 2011) and some only evaluation of the number of the stained cells (de Vicente et al., 2017). The latter one was chosen to be used here, as it was simple to perform. Furthermore, it does not study the phenomenon with two parameters, which would have quite likely lead to the same outcome.

6.2.1.2 Tools for quantification of immunostaining

In this study, most of the work for quantifying the immunostaining was done by manual tools. A machine-learning-based method could have saved a significant amount of time, had a suitable tool been available. However, currently there apparently are no suitable tools, as the current machine-learning-utilizing histological tools require quite homogenous tissue to analyze. The stained samples in this thesis had quite large amount of unwanted - and nevertheless stained - matter from seminal vesicles. The heterogeneity of the tissue often renders the images useless for computational tools. Another major obstacle is that most machine-learning-based methods require a lot of data, as a part of the data set is first used for training before the rest of the data can be analyzed (Bartaula, 2017).

ImmunoRatio-software was used here to analyze P-S6-whole-cell-staining in neoplasia model samples and later was it was tested for nuclear Ki-67-staining analysis as well. The proliferation marker Ki-67 is one of the recommended targets of the ImmunoRatio, but the mouse prostate tissue was not quite optimal for ImmunoRatio due to the glandular structure. When the ImmunoRatio and manual counting were compared within a same area, the ImmunoRatio proved to be over one minute faster per sample (including image cropping), but the manual counting seemed to be the more accurate way of quantification – especially when it is routinely carried out by two separate inspectors. With manual counting, between 3 and 25 percentage units more Ki-67 expressing nuclei were detected in the samples compared to the ImmunoRatio-analysis. The difference between the two methods may originate from the size of the nuclei because the ImmunoRatio uses surface areas, which are dichotomized being either brown or blue, whereas manual counting relies on the number of brown and blue nuclei. Previously, with P-S6 quantification, saturation of images first seemed to improve the ImmunoRatio-analysis results.

Genotypes were not known when the images were used for quantifying the staining. However, in the primary prostate cancer model, for example, the lateral prostate was visibly different in some samples (likely due to intraepithelial neoplasm). This means that looking at the tissue structure and nuclei size can already provide information, which would lead to the conclusion that the assessing of staining was not actually completely blinded.

6.3 Analysis of expression of miR-32 in primary prostate cancer model

In addition to immunohistochemistry, qPCR experiments were also performed on samples with the MiR-32/Myc-genotype. The first step towards the qPCR was the extraction of the RNA. The RNA extraction kit buffers consisted of substances such as ethanol and the guanidine isocyanate (GITC). However, the extraction product may have had contained GITC as a contaminant, which is known to alter, for example, the 260/230 ratio (Matlock, 2015). An example of the effect of the GITC on absorbance spectra can be seen in Figure 27. However, according to the manufacturer, the GITC residue should not prevent the use of the extracted RNA.

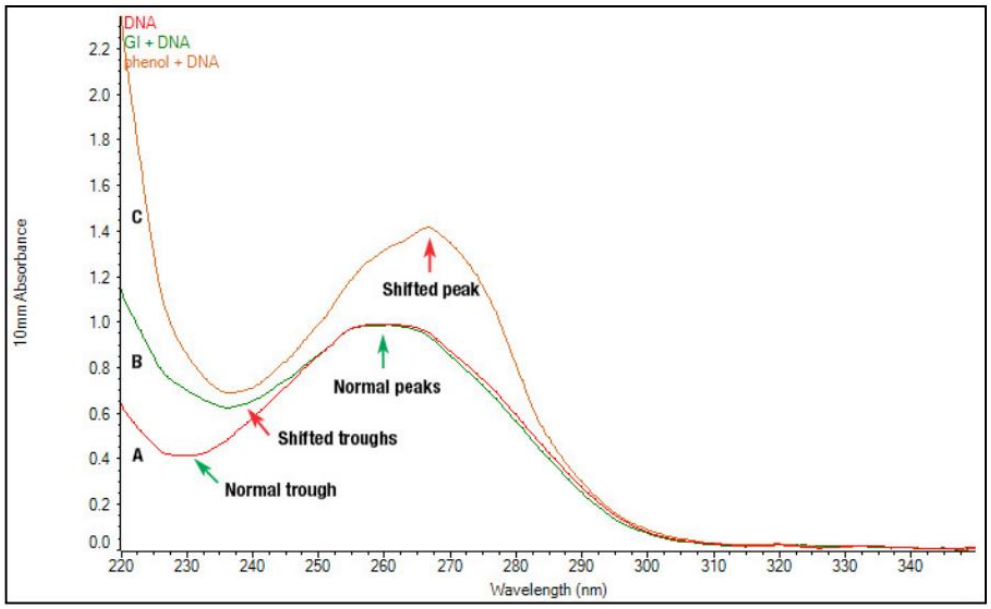

Figure 27. Contaminants affect nucleic acid spectra. Guanidine isocyanate (line B in the image) residue shifts the absorbance near 230-240 nm area, which should be an area of relatively low absorbance if the RNA/DNA sample is pure. Image from (Matlock, 2015).

During RNA extraction process, there may have been different centrifugal forces for different sample sets, which is possibly an error source. Because two other people were using the same centrifuge equipment from time to time when the RNA extraction was performed, it may be that both the RPM (rotations per minute) and RCF/G-force (relative centrifugal force) units may have been used during one session. This is a problem as, for example, 16 000 g is not the same as 16 000 RPM, but instead with a centrifuge with a rotor with a 10-cm-long radius it is roughly 12 000 RPM. The formula for conversion from RCF/G-force to *RPM is RCF = 1.12 x Radius x (rpm/1000)*^{2}. The protocol for RNA extraction advised to use the maximum speed at four different steps, so 16 000 g was supposed to be used in these cases, but if the unit had been rpm by mistake, the speed would have been significantly lower. This could have affected at least the uniformness of the protocol for different samples.

The volume of the extracted product was set to 20µl for every sample by adding dH_20. The extracted product is therefore not the strongest possible, but instead the altered volume and the concentration was thought to be reasonable for the needs of the cDNA synthesis.

The cDNA was synthesized first with only two samples, and only after this the rest of the set (18 samples) was handled. This could be considered a mistake, as the cDNA from two separate sessions of PCR are not necessarily comparable. The reason for using a small, two-sample-set as the first samples was to make sure that the procedure would be carried out without problems when the rest of the samples were in line. Instead of a few samples as a test set, other non-valuable samples from other sources could have and should have been used. The qPCR experiment with the SYBR Green -fluorophores and Myc-primers confirmed the Myc-expression in the samples. This was crucial for the assumption of having cancer-like conditions in the mouse prostate, since the Myc overexpression was the major driving force of the tissue alteration.

The Myc-expression was normalized with the β-Actin as a housekeeping gene. Using the Pfaffl method for data normalization produced a little incoherent set of data, but the ratio of calculated starting quantities (SQ ratio) seemed to provide more reasonable results, especially when compared to the AGE image results. As an example of the variability between the two methods, the sample 192 had relative value of either 1 or 3 depending on the calculation method. Pfaffl method did not seem to be completely reliable, so a ratio of starting quantities was used for analysis.

There would have been other methods for qPCR data processing such as the Livak method (the $2^{-\Delta\Delta CT}$ method), but they had unmet assumptions. For example, the Livak method requires assuming equal efficiencies.

6.3.1.1 qPCR data analysis and validation

To interpret the results of the qPCR for Myc, several steps of data analysis and analysis validation was performed first.

The optimal fitting of a linear line to the standard curve was carried out by removing outliers, in this case many of the most diluted standard samples. Even with this maneuver, the efficiency and the R^2-value were not optimal. Abnormal efficiency means that the pipetting process might have had faults and a poor R^2-value will lead to a decreased ability to read sample concentrations from the linear standard curve. The qPCR assay was repeated several times to achieve an outcome near optimal, but the result presented here was the best.

Optimizing the reaction conditions and re-designing of the primers could improve the efficiency. For example, temperature and primer concentrations could be altered in some cases and suitable

software could be used to assess, whether the current design of the primers allows formation of primer-dimers or not. Primer-dimers can form, for example, because of complementary 3' end sequences in forward and reverse primers. Primer-dimers in qPCR process can be detected with a melt peak graph (Bio-Rad Laboratories, 2006).

When the melt peak graphs were analyzed, they were found to consist of two different peaks (see Figure 28) even though the agarose gel after electrophoresis contained only the expected product bands. Therefore, it is likely, that the byproduct was amplified in very small amount and in a late stage when compared to the main product. There are multiple possible interpretations for two peaks in a melt peak graph. For example, a contamination, primer-dimers (Bio-Rad Laboratories, 2006), and melting (denaturation) of the double-stranded DNA product in different steps (Yongjiang Li, 2016) are possible causes for the phenomenon. The latter means that if there were, for example, a very GC-rich area in the Myc gene, it might be melting only after other, more uniform areas of the amplified DNA product (Yongjiang Li, 2016). In this way, a melting process with two major steps could produce two peaks in the melt peak graph (Bio-Rad Laboratories, 2006). Even though not likely, for example, Figure 28A from qPCR for MYC could show a primer-dimer-caused peak with lower melting point.

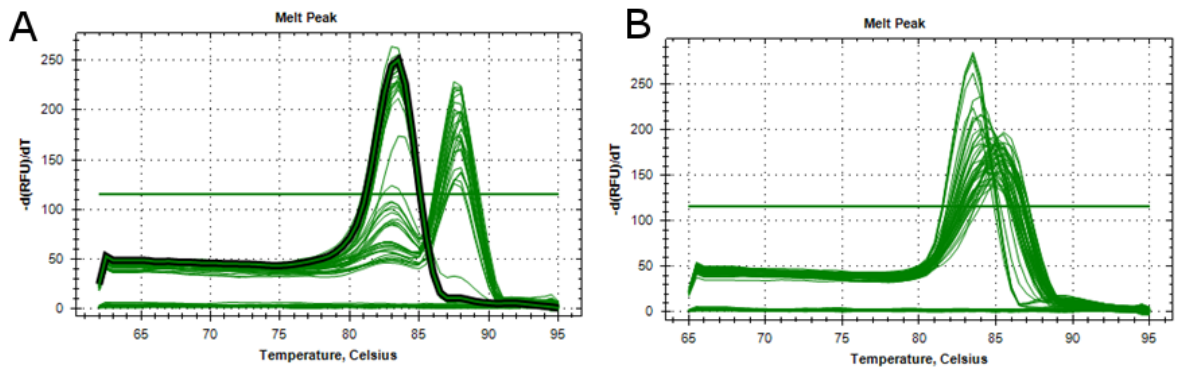

Figure 28. Shown in panel A (left), is the melt peak graph from qPCR experiment for the Myc gene (miR-32 +/- Myc +/- genotype). Two peaks can be seen in the graph at +83°C and +87°C temperatures. Shown in panel B (right), is the melt peak for housekeeping gene b-Actin assessment with qPCR. The melt peak graph has two overlapping peaks at +83°C and +86°C temperatures.

The products of the qPCR were verified with agarose gel electrophoresis technique. The image, which was obtained from gels containing Myc-DNA, was quite dim, whereas the β-Actin-bands in the other gel were quite easy to see under similar settings. This could be due to some unknown difference in setup (the imaging device was under repair between the two experiments) or simply because β-Actin is likely more expressed than Myc. To alleviate the dimness of the gel images,

contrast and brightness were added. The image manipulation was performed equally for every image, so it should not be an error source.

6.3.2 Analysis of miR-32 expression

The TaqMan assay with miR-32-targeting probes confirmed the presence of miR-32 in the used mice generations, F5 and F7. As well as confirmation of presence of Myc in the samples, this was highly important for the study design, since the miR-32 expression by ARR2PB-construct was assumed to be still active in the samples. Thus, at least the miR-32/Myc was shown to be valid by genotype.

The normalized level of miR-32 in the samples was relatively low when compared to previously obtained results from earlier generations of the same mice (Latonen, 2014). However, the genotyping experiment demonstrates that the ARR2PB-miR32-transgene system is still functional even seven generations after it was first activated. The used samples were obtained from the ventral lobe of the mouse prostate, since the miR32 expression is highest in the ventral lobe.

The TaqMan-assay appeared to have a problem with a sub-optimal experiment length. This means, that the amplification process was cut out because only 39 repeats were programmed into the system. Instead, for example, 49 repeats could have been used as was done in a guidebook source (Bio-Rad Laboratories, 2006). The miR-32-expression was normalized with reference gene, RNU6B expression data. The RNU6B expression data was obtained from an external series of experiments.

6.3.3 Final words

6.3.3.1 What could have been done otherwise?

The experimental part of the thesis mostly followed its schedule and was finished by the end of August 2017, roughly five months after its beginning. This proved to be only just enough of time for the laboratory work, as, for example, unexpected occasions of equipment breaking down and being repaired took a substantial amount of time. With more time, carrying out more experiments would have been possible. The next section gives an overview of what could have been done additionally.

Firstly, the failed experiments could have been repeated in an optimal situation if extra samples would have been available. The experiments to be repeated would have been immunostaining against mitotic marker P-H3 in normal epithelium (since a part of data was excluded) and against the second proliferation marker, PCNA, in primary prostate cancer model samples.

Also, repeating several non-optimal experiments could have improved the certainty of conclusions which were drawn from the data. The analysis of apoptotic marker cleaved caspase-3 in normal epithelium was quite likely slightly biased. A repeat would confirm, if there was a bias or not. The list of potential experiment to repeat would include also the markers cleaved caspase-3 and Ki-67 in

primary prostate cancer model (optimal conditions would produce optimal staining quality), analysis of MYC expression with qPCR (to produce a PCR reaction without byproducts) and miR32 analysis with TaqMan assay (length of the TaqMan assay experiment would have been more optimal with 10 or so more cycles).

As implicated before, the indirect immunohistochemistry with HRP/DAB-system was a major part of the thesis. In addition to the used IHC methods, also in situ -hybridization could have been used to detect e.g. miR32 in the samples, since in situ hybridization targets specific nucleotide sequences in cells. Detecting micro-RNA 32 could have been used as an additional confirmation that the transgene for miR32 was functional. However, in situ -hybridization technique requires quite a lot of optimization before the optimal conditions are found (Alanen, 2014).

Also, in the RNA extraction phase, there could have been more purification steps to get rid of the contaminating GITC. Still, the protocol has been tested extensively by PreAnalytix GmbH before commercializing, and the protocol for the kit was followed to the point (disregarding the previous alterations to the protocol), so it is uncertain whether additional steps would have been beneficial. Also, other extraction protocols and kits could have been compared to the PAXgene-extraction kit to find a protocol with best purity and/or yield.

The workflow for Myc-gene assessment in primary prostate cancer model samples consisted of RNA extraction, cDNA synthesis by reverse transcription and finally, the qPCR experiment. The qPCR steps were carried out each time by first using reverse transcription and then separately performing qPCR. Yet, a combined RT-qPCR-method could have been used to eliminate some possible error sources.

As one can notice, the PTEN-heterozygote background of the samples was not confirmed in this thesis. This is, because the neoplasia served as an additional source of data for an article for a scientific journal, and therefore a major part of the PTEN-related work and other experiments had already been performed.

Finally, the machine learning -based methods could have possibly assisted with the quantificational part of this thesis, but only if the testing set had been pre-performed with images of similar tissue and the amount of data collected in this thesis had been much larger. The relatively simple Immunoratio software is still an unintelligent software, but other methods will quite certainly be developed further.

6.3.3.2 What's next?

In human prostate, microRNA-32 is known to be regulated by the androgens (Waltering et al., 2011), and it may have an important regulatory role in prostate cancer (Jalava et al., 2012). MiR-32 used

with or without other micro-RNAs could be a promising marker to use in diagnostics to reach a better outcome than by using only the current PSA- and Gleason score-based diagnostics method. In addition to the short, non-coding RNAs such as miRNAs, also long non-coding RNAs are being studied for their marker potential especially for detecting CRPC (Ylipää et al., 2015). The more accurate the diagnostics is, the better treatment decisions can be made – the decision could be, for example, whether radical prostatectomy is performed or not. Therefore, studying both miRNAs and lncRNAs together might produce a panel of valuable markers.

In addition to marker potential, the miRNAs could also be the therapeutic targets themselves (van Rooij, Purcell, & Levin, 2012). A therapeutic application could even be a miRNA-mimicking synthetic RNA, which already has been studied for replenishing certain miRNAs lost under disease conditions (van Rooij et al., 2012). Before therapeutically promising putative miRNA-related strategies can be considered for therapeutic applications, several severe pharmacological problems still need to be solved.

There are challenges, for example, with the delivery of a sufficient therapeutic amount, the rapid degradation of RNAs and the safety of the technique (Ekins & Xu, 2009). Delivery could be facilitated by, for example, nanoparticle conjugation and liposomal coating or with a viral vector (Ekins & Xu, 2009; van Rooij et al., 2012). Degradation could be slowed down by chemical modification of the structure and well-done sequence selection (Ekins & Xu, 2009). Safety problems can include activation of the innate immune system and possible hybridization to partially non-complementary sequences (Ekins & Xu, 2009). Even selection of canonical sequences has been shown to have off-target effects (Ekins & Xu, 2009). Too large quantities of exogenous miRNA can also harm endogenous miRNA processing, especially in the liver and therefore induce toxicity (Ekins & Xu, 2009). If several miRNAs are used together for better impact, their joint adverse effects need to be considered as well.

All in all, legion of studies are still needed before the current knowledge or non-coding RNAs can be used for medical applications for prostate cancer. In this way, the study with the three mouse prostate models presented in this thesis pave the way for further research.

7. Conclusions

7.1 Summary

To conclude, the study showed, that in normal mouse prostate epithelium (in age group of 3-6 months), presence of miR-32 had very little effect. The same results applied for the neoplasia model, the PTEN heterozygote sample series, where mice were 10-11 months old. The samples with miR-32/Myc were representing the state of a primary cancer in mouse prostate and showed that presence of miR-32 in the samples did not have significant effect compared to the miR-32-negative samples in the age group of 3 months old mice.

To summarize the results of this thesis, Table 2 shows most of the results together.

Table 2. Summary of the major results of the laboratory work for the thesis.

miR-32 series: normal epithelium	**P-H3**	**Cleaved caspase-3**	**PCNA**	**P-S6**
	Roughly 0.5%–1.5% of P-H3-positive nuclei with a quite large variation. No significant differences between miR32-positive and -negative group. Part of the data was excluded.	The quantification was likely biased and results were excluded.	PCNA expression ranged from 60–80% of nuclei. Statistically significant differences between the groups were not found.	Evaluation by estimation of staining in each sample lobe: In the miR-32-positive group, 75% of cells were P-S6-positive in dorsal lobe, 50% in lateral and 62.5% in ventral. In the miR-32-negative group, the respective values were 60%, 80% and 60%.
PTEN/MiR32-series: neoplasia model	**P-H3**	**Cleaved caspase-3**	**PCNA**	**P-S6**
	~3% of P-H3-positive nuclei. No difference between miR32-negative and -positive groups.	~ 1.5% of cleaved caspase 3 -positive nuclei. No difference between miR32-neg. and -pos. groups.	>90% of PCNA-positive nuclei in both miR32-negative and -positive groups.	Immunoratio-analysis: on average, there were 73.1% of P-S6-positive cells in the miR-32-positive group and 84.1% in miR-32-negative group, but different is not statistically

				significant.
MYC/miR-32-series (IHC): primary prostate cancer model	**P-H3**	**Cleaved caspase-3**	**PCNA**	**Ki-67**
	Myc-positive groups have over 5% of P-H3-positive nuclei and Myc-negative close to zero, but miR-32 status does not have any effect.	Staining process flawed by a wrong buffer. The outcome was weak, and only few cleaved caspase-3 -positive nuclei were present. No major differences between miR32-negative and -positive groups.	Staining process with a wrong buffer. The staining outcome was too faint to be analyzed.	Proliferation marker Ki-67 was present in Myc-positive sample groups. In these groups 13–15% of nuclei were Ki-67-positive. MiR-32 had no effect. Staining process was flawed by a wrong buffer.
MYC/miR-32-series (qPCR)	Confirmed Myc expression in Myc-positive groups. These groups were from 3 months old mice. Some samples were from parental line 036 and some from 470, which have the ARR2PB-element insertion at different location in genome. Expression in both these groups was confirmed.			
MYC/miR-32-series (TaqMan assay)	Confirmed miR-32-expression in miR-32-positive groups. These groups were either from fifth or seventh filial generation.			

8. References

Aakula, A., Kohonen, P., Leivonen, S., Mäkelä, R., Hintsanen, P., Mpindi, J., Martens-Uzunova, E., Aittokallio, T., Jenster, G., Perälä, M., Kallioniemi, O. & Ostling, P. (2016). Systematic Identification of MicroRNAs That Impact on Proliferation of Prostate Cancer Cells and Display Changed Expression in Tumor Tissue". European Urology, 69(6), 1120-1128.

Abate-Shen, C., & Shen, M. M. (2010). Molecular genetics of prostate cancer. Genes & Development, 14(19), 2410-2434.

Alanen, O. (2014). Expression of miR32, ki-67, btg2 and pten in transgenic mouse prostate tissue (Thesis for Bachelor's Degree).

Andriani, F., Nan, B., Yu, J., Li, X., Weigel, N. L., McPhaul, M. J., . . . Marcelli, M. (2001). Use of the probasin promoter ARR2PB to express bax in androgen receptor-positive prostate cancer cells. Journal of the National Cancer Institute, 93(17), 1314-1324.

Applied Biosystems. (2006). TaqMan® MicroRNA assays protocol (PDF) Applied Biosystems.

Bartaula, J. (2017). Classification of lymph node metastases in breast cancer with features from tissue images using machine learning techniques (Master's thesis).

Bio-Rad Laboratories, I. (2006). Real-time PCR application guide.

Cameron, D. E., Bashor, C. J., & Collins, J. J. (2014). A brief history of synthetic biology. Nature Reviews Microbiology, 12(5), 381-390.

Carvalhal, G. F., Daudi, S. N., Kan, D., Mondo, D., Roehl, K. A., Loeb, S., & Catalona, W. J. (2010). Correlation between serum prostate-specific antigen and cancer volume in prostate glands of different sizes. Urology, 76(5), 1072-1076.

Catto, J. W., Alcaraz A., . . . Visakorpi, T. (2011). MicroRNA in prostate, bladder, and kidney cancer: A systematic review. European Urology, 59(5), 671-681.

Chaisuparat, R., Limpiwatana, S., Kongpanitkul, S., Yodsanga, S., & Jham, B. C. (2016). The Akt/mTOR pathway is activated in verrucous carcinoma of the oral cavity. Journal of Oral Pathology & Medicine: Official Publication of the International Association of Oral Pathologists and the American Academy of Oral Pathology, 45(8), 581-585.

Costello, L. C., Franklin, R. B., & Feng, P. (2005). Mitochondrial function, zinc, and intermediary metabolism relationships in normal prostate and prostate cancer. Mitochondrion, 5(3), 143-153.

Culig, Z., & Santer, F. R. (2014). Androgen receptor signaling in prostate cancer. Cancer Metastasis Reviews, 33(2), 413-427.

Damber, J. E., & Aus, G. (2008). Prostate cancer. Lancet (London, England), 371(9625), 1710-1721.

Daniel, R., Wu, Q., Williams, V., Clark, G., Guruli, G., & Zehner, Z. (2017). A panel of MicroRNAs as diagnostic biomarkers for the identification of prostate cancer. International Journal of Molecular Sciences, 18(6).

De Bruyn, R., Bollen, R., & Claessens, F. (2011). Identification and characterization of androgen response elements. Methods in Molecular Biology (Clifton, N.J.),

de Vicente, J. C., Pena, I., Rodrigo, J. P., Rodriguez-Santamarta, T., Lequerica-Fernandez, P., Suarez-Fernandez, L., . . . Garcia-Pedrero, J. M. (2017). Phosphorylated ribosomal protein S6 correlation with p21 expression and inverse association with tumor size in oral squamous cell carcinoma. Head & Neck, 39(9), 1876-1887.

Di Cristofano, A., Pesce, B., Cordon-Cardo, C., & Pandolfi, P. P. (1998). Pten is essential for embryonic development and tumour suppression. Nature Genetics, 19(4), 348-355.

Egervari, G., Mark, A., Hajdu, M., Barna, G., Sapi, Z., Krenacs, T., . . . Sebestyen, A. (2011). Mitotic lymphoma cells are characterized by high expression of phosphorylated ribosomal S6 protein. Histochemistry and Cell Biology, 135(4), 409-417.

Ekins, S., & Xu, J. J. (2009). Drug efficacy, safety, and biologics discovery: Emerging technologies and tools. John Wiley & Sons.

Ellwood-Yen, K., Graeber, T. G., Wongvipat, J., Iruela-Arispe, M. L., Zhang, J. F., Matusik, R., . . . Sawyers, C. L. (2003). Myc-driven murine prostate cancer shares molecular features with human prostate tumors. Cancer Cell, 4(3), 223-238.

Fulda, S. (2014). Molecular pathways: Targeting inhibitor of apoptosis proteins in Cancer—From molecular mechanism to therapeutic application. Clinical Cancer Research, 20(2), 289-295.

Geng, C., Kaochar, S., Li, M., Rajapakshe, K., Fiskus, W., Dong, J., . . . Mitsiades, N. (2017). SPOP regulates prostate epithelial cell proliferation and promotes ubiquitination and turnover of c-MYC oncoprotein. Oncogene, 36(33), 4767-4777.

Hanahan, D., & Weinberg, R. A. (2011). Hallmarks of cancer: The next generation. Cell, 144(5), 646-674.

Henzler, C., Li, Y., Yang, R., McBride, T. A., Ho, Y., Sprenger, C., . . . AUID, D. S. (2016). Truncation and constitutive activation of the androgen receptor by diverse genomic rearrangements in prostate cancer. Nature Communications, 7(13668).

Hu, J., Wang, G., & Sun, T. (2017). Dissecting the roles of the androgen receptor in prostate cancer from molecular perspectives. Tumour Biology: The Journal of the International Society for Oncodevelopmental Biology and Medicine, 39(5)10.

Iwenofu, O. H., Lackman, R. D., Staddon, A. P., Goodwin, D. G., Haupt, H. M., & Brooks, J. S. (2008). Phospho-S6 ribosomal protein: A potential new predictive sarcoma marker for targeted mTOR therapy. Modern Pathology: An Official Journal of the United States and Canadian Academy of Pathology, Inc, 21(3), 231-237.

Jalava, S. E., Urbanucci, A., Latonen, L., Waltering, K. K., Sahu, B., Janne, O. A., . . . Visakorpi, T. (2012). Androgen-regulated miR-32 targets BTG2 and is overexpressed in castration-resistant prostate cancer. Oncogene, 31(41), 4460-4471.

Juríková, M., Danihel, Ľ., Polák, Š., & Varga, I. (2016). Ki67, PCNA, and MCM proteins: Markers of proliferation in the diagnosis of breast cancer. Acta Histochemica, 118(5), 544-552.

Kap, M., Smedts, F., Oosterhuis, W., Winther, R., Christensen, N., Reischauer, B., . . . Riegman, P. (2011). Histological assessment of PAXgene tissue fixation and stabilization reagents. Plos One, 6(11), e27704.

Kaushal, V., Herzog, C., Haun, R. S., & Kaushal, G. P. (2014). Caspase protocols in mice. Methods in Molecular Biology (Clifton, N.J.), 1133, 141-154.

Kim, J., Roh, M., Doubinskaia, I., Algarroba, G. N., Algarroba, G. N., Eltoum, I. E., & Abdulkadir, S. A. (2012). A mouse model of heterogeneous, c-MYC-initiated prostate cancer with loss of pten and p53. Oncogene, 31(3), 322-332.

Kim, S. W., Roh, J., & Park, C. S. (2016). Immunohistochemistry for pathologists: Protocols, pitfalls, and tips. Journal of Pathology and Translational Medicine, 50(6), 411-418.

Lagos-Quintana, M., Rauhut, R., Lendeckel, W., & Tuschl, T. (2001). Identification of novel genes coding for small expressed RNAs. Science (New York, N.Y.), 294(5543).

Latonen, L. (2014). Modelling human prostate cancer in mice - transgenic miR-32 expression in mouse prostate. Project report, pathology training program in disease modeling. (Project report). University of Tampere.

Latonen, L., Scaravilli, M., Gillen, A., Hartikainen, S., Zhang, F., Ruusuvuori, P., . . . Visakorpi, T. (2017). In vivo expression of miR-32 induces proliferation in prostate epithelium. The American Journal of Pathology, 187(11), 2546-2557.

Leite, K. R. M., Tomiyama, A., Reis, S. T., Sousa-Canavez, J. M., Sañudo, A., Camara-Lopes, L. H., & Srougi, M. (2013). MicroRNA expression profiles in the progression of prostate cancer—from high-grade prostate intraepithelial neoplasia to metastasis. Urologic Oncology: Seminars and Original Investigations, 31(6), 796-801.

Lilja, H., Ulmert, D., & Vickers, A. J. (2008). Prostate-specific antigen and prostate cancer: Prediction, detection and monitoring. Nat Rev Cancer, 8(4), 268-278.

Lipman, N. S., Jackson, L. R., Trudel, L. J., & Weis-Garcia, F. (2005). Monoclonal versus polyclonal antibodies: Distinguishing characteristics, applications, and information resources. ILAR Journal, 46(3), 258-267.

Liu, C., Liu, R., Zhang, D., Deng, Q., Liu, B., Chao, H. P., . . . Tang, D. G. (2017). MicroRNA-141 suppresses prostate cancer stem cells and metastasis by targeting a cohort of pro-metastasis genes. Nature Communications, 8(14270).

Magnuson, B., Ekim, B., & Fingar, D. C. (2012). Regulation and function of ribosomal protein S6 kinase (S6K) within mTOR signalling networks. The Biochemical Journal, 441(1), 1-21.

Malcomson, F. C., Willis, N. D., McCallum, I., Xie, L., Lagerwaard, B., Kelly, S., . . . Mathers, J. C. (2017). Non-digestible carbohydrates supplementation increases miR-32 expression in the healthy human colorectal epithelium: A randomized controlled trial. Molecular Carcinogenesis, 56(9), 2104-2111.

Matlock, B. (2015). Technical note 52646: Assessment of nucleic acid purity. (Technical). Thermo Fisher Scientific.

miRBase. (2016). miRBase: Hsa-mir-32. Retrieved from http://mirbase.org/cgi-bin/mirna_entry.pl?acc=MI0000090.

Montironi, R., Mazzucchelli, R., Algaba, F., & Lopez-Beltran, A. (2000). Morphological identification of the patterns of prostatic intraepithelial neoplasia and their importance. Journal of Clinical Pathology, 53(9), 655-665.

NCBI. (2017). Myc myelocytomatosis oncogene [mus musculus (house mouse)] gene ID: 17869. Retrieved from https://www.ncbi.nlm.nih.gov/gene/17869.

Ng, R., Hussain, N. A., Zhang, Q., Chang, C., Li, H., Fu, Y., . . . Xu, F. (2017). miRNA-32 drives brown fat thermogenesis and trans-activates subcutaneous white fat browning in mice. Cell Reports, 19(6), 1229-1246.

Oliveira, D. S., Dzinic, S., Bonfil, A. I., Saliganan, A. D., Sheng, S., & Bonfil, R. D. (2016). The mouse prostate: A basic anatomical and histological guideline. Bosnian Journal of Basic Medical Sciences, 16(1), 8-13.

Perez-Cadahia, B., Drobic, B., & Davie, J. R. (2009). H3 phosphorylation: Dual role in mitosis and interphase. Biochemistry and Cell Biology, 87(5), 695-709.

Remáková, M., Skoda, M., Faustová, M., Vencovský, J., & Novota, P. (2013). Validation of RNA extraction procedures focused on micro RNA expression analysis. Folia Biologica, 59(1), 47.

Robinson, D. R., Wu, Y., Lonigro, R. J., Vats, P., Cobain, E., Everett, J., . . . Chinnaiyan, A. M. (2017). Integrative clinical genomics of metastatic cancer. Nature, 548(7667), 297-303.

Sandberg, R., Neilson, J. R., Sarma, A., Sharp, P. A., & Burge, C. B. (2008). Proliferating cells express mRNAs with shortened 3' untranslated regions and fewer microRNA target sites. Science (New York, N.Y.), 320(5883), 1643-1647.

Shen, J., & Hung, M. (2015). Signaling-mediated regulation of MicroRNA processing. Cancer Research, 75(5), 783-791.

Scholzen, T., & Gerdes, J. (2000). The Ki-67 protein: From the known and the unknown. Journal of Cellular Physiology, 182(3), 311-322.

Shappell, S. B., Thomas GV, Roberts RL, Michael, M., Rubin MA, Humphrey PA, . . . Barrios R. (2004). Prostate pathology of genetically engineered mice: Definitions and classification. The consensus report from the Bar Harbor meeting of the mouse models of human cancer consortium prostate pathology committee (2001). Cancer Research, 64(6), 2270-2305.

Song, M. S., Salmena, L., & Pandolfi, P. P. (2012). The functions and regulation of the PTEN tumour suppressor. Nature Reviews. Molecular Cell Biology, 13(5), 283-296.

Steven, A., Lowe, J. S., & Young, B. (2002). Wheater's basic histopathology: A color atlas and text. Churchill Livingstone.

Sun, Y., Cong, L., Zhong, X., Ma, Y., Luo, P., Liu, M., . . . Liu, X. (2017). Decreased expression of miR-32 is associated with the clinical outcome of non-small cell lung cancer patients. International Journal of Clinical and Experimental Pathology, 10(5), 6021-6028.

Suomen Syöpärekisteri. (2016). Suomen syöpärekisteri (database): The detected new prostate cancer cases by year (2010-2015). Retrieved from https://tilastot.syoparekisteri.fi/syovat.

Tapia, C., Kutzner, H., Mentzel, T., Savic, S., Baumhoer, D., & Glatz, K. (2006). Two mitosis-specific antibodies, MPM-2 and phospho-histone H3 (Ser28), allow rapid and precise determination of mitotic activity. The American Journal of Surgical Pathology, 30(1), 83-89.

Thermo Fisher Scientific. (2017). IVD DATA SHEET rev 012210C: Ki-67 (rabbit monoclonal). Retrieved from https://assets.thermofisher.com/TFS-Assets/APD/Specification-Sheets/D12536~.pdf

Thermo Fisher Scientific Inc. (2015). Real-time PCR handbook.

Toivanen, R., & Shen, M. M. (2017). Prostate organogenesis: Tissue induction, hormonal regulation and cell type specification. Development (Cambridge, England), 144(8), 1382-1398.

Trotman, L. C., Niki, M., Dotan, Z. A., Koutcher, J. A., Di Cristofano, A., Xiao, A., . . . Pandolfi, P. P. (2003). Pten dose dictates cancer progression in the prostate. PLOS Biology, 1(3), e59.

van Rooij, E., Purcell, A. L., & Levin, A. A. (2012). Developing microRNA therapeutics. Circulation Research, 110(3), 496-507.

Waltering, K. K., Porkka, K. P., Jalava, S. E., Urbanucci, A., Kohonen, P. J., Latonen, L. M., . . . Visakorpi, T. (2011). Androgen regulation of micro-RNAs in prostate cancer. The Prostate, 71(6), 604-614

Warford, A., Akbar, H., & Riberio, D. (2014). Antigen retrieval, blocking, detection and visualisation systems in immunohistochemistry: A review and practical evaluation of tyramide and rolling circle amplification systems. Methods (San Diego, Calif.), 70(1), 28-33.

Watson, P., Arora, V., & Sawyers, C. (2015). Emerging mechanisms of resistance to androgen receptor inhibitors in prostate cancer. Nature Reviews Cancer, 15(12), 701-711.

Wise, H. M., Hermida, M. A., & Leslie, N. R. (2017). Prostate cancer, PI3K, PTEN and prognosis. Clinical Science (London, England: 1979), 131(3), 197-210.

Xia, W., Zhou, J. Y., Luo, H. B., Liu, Y. Z., Peng, C. C., Zheng, W. L., & Ma, W. L. (2017). MicroRNA-32 promotes cell proliferation, migration and suppresses apoptosis in breast cancer cells by targeting FBXW7. Cancer Cell International, 17(1).

Ylipää, A., Kivinummi, K., Kohvakka, A., Annala, M., Latonen, L., Scaravilli, M., . . . Nykter, M. (2015). Transcriptome sequencing reveals PCAT5 as a novel ERG-regulated long noncoding RNA in prostate cancer. Cancer Research, 75(19), 4026-4031.

Yongjiang Li. (2016). 6 tips to improve qPCR. Retrieved from https://sciencellonline.com/blog/6-tips-to-improve-qpcr-part-2-of-3/.

Zhang, Y., & Reinberg, D. (2001). Transcription regulation by histone methylation: Interplay between different covalent modifications of the core histone tails. Genes & Development, 15(18), 2343-2360.

9. Supplementary material

9.1 Supplementary tables

All sample and tissue section slide numbers (with their respective antibodies of choice) are listed below in Table 3.

Table 3. Sample and slide numbers for all tissue sections used in the experimental part of the thesis.

MICE SAMPLES:						
Neoplasia model (Pten/miR-32) samples						
Sample code	Cleaved Caspase 3	PCNA	P-H3	P-S6		
Lat-186_PtenX036-011	51	54	56	50		
Lat-186_Ptenx036-14	36	29	32	35		
Lat-186_PTENX036-15	41	44	45	39		
Lat-186_PTENX036-20	12	11	8	14		
Lat-186_PTENX036-021	80	83	81	78		
LAT-186_PTENX036-032	63	65	63	60		
LAT-186_PTENX036-033	42	44	47	41		
Lat-186_PTENX036-34	69	71	72	68		
Lat-186_Ptenx036-039	71	69	66	72		
Lat-186_Ptenx036-040	39	42	44	38		
Lat-186_Ptenx036-042	59	56	54	60		
LAT-186_PTENX036-068	57	53	56	59		
Age: 10-11 months						
Parental line 036, miR-32 transgene activated 3 generations ago (F3)						
Normal epithelium samples						
DNA code	p-H3	PCNA	cleaved Casp-3	p-S6		
361	69	71	72	74		
362	72	76	77	79		
363	12,57, 110	11, 56, 111	9, 54, 113	8, 53, 114		
364	45, 86	44, 87	42, 89	41, 90		
365	44	42	41	39		
366	41	39	38	36		
367	19	17	16	14		
399	44	42	41	39		
400	44	38	36	39		
401	27	29	30	32		
402	68	66	65	63		
403	63	54	56	57		
404	47	48	44	45		
Age: half were 3 months, other half 6 months						
Parental line 036, miR-32 transgene activated 2 generations ago (F2)						

Primary prostate cancer model: miR-32/Myc-series (for IHC and qPCR)						
Mouse number	RNA-tube number	Ki-67	P-H3	Casp-3	PCNA	
164	3	65	66	68	69	
179	3	62	63	65	66	
180	3	89	90	92	93	
181	4	89	90	92	93	
182	3	89	90	92	93	
184	2	29	30	32	33	
189	4	122	123	125	126	
190	3	65	66	68	69	
192	3	77	78	80	81	
1356	2	62	63	65	66	
1357	2	29,119	30,1	32,1	33,1	
1358	3	62	63	65	66	
1359	3	89	90	92	93	
1360	3	86	87	89	90	
1361	2	56	57	59	60	
1362	3	35	36	38	39	
1363	2	56	57	59	60	
1363	1	17	18	20	21	
1364	1	26,62	27,6	29,7	30,7	
1365	2	38,89	39,9	41,9	42,9	
Age: Hi-Myc mice are 3 months old. Other mice are from parental line 036 at generation F7,						
except samples 179-184, which are from parental line 470 generation F5. Parental lines 036 and 470						
have different copy numbers and are not located at the same site in the genome.						
Primary prostate cancer model: miR-32/Myc-series (TaqMan assay)						
Both groups from ventral prostate						
Group 470	Group 036					
288	280					
289	281					
303	282					
304	283					
305	293					
306	294					
307	295					
308	296					
309	297					
310	321					
311	322					
342	323					

358	324					
359	325					
360	326					
	327					
	347					
	348					

Below, is the supplementary Table 4, which shows the absorbance measurements from the extracted RNA.

Table 4. Absorbance and absorbance ratios from the extracted RNA.

Sample ID	**Nucleic acid concentration**	**Unit**	**A260 (Abs)**	**A280 (Abs)**	**260/280**	**260/230**	**Sample Type**
164	118,7	ng/µl	2,967	1,348	2,2	0,33	RNA
179	180,4	ng/µl	4,509	2,126	2,12	0,77	RNA
180	30,7	ng/µl	0,767	0,337	2,28	0,21	RNA
181	115,8	ng/µl	2,895	1,339	2,16	0,65	RNA
182	129,1	ng/µl	3,227	1,502	2,15	0,53	RNA
184	364,2	ng/µl	9,105	4,278	2,13	1,16	RNA
189	114,6	ng/µl	2,864	1,343	2,13	0,41	RNA
190	126	ng/µl	3,151	1,515	2,08	0,6	RNA
192	271,1	ng/µl	6,777	3,158	2,15	1,01	RNA
1356	96,1	ng/µl	2,402	1,164	2,06	0,36	RNA
1357	51,8	ng/µl	1,295	0,603	2,15	0,34	RNA
1358	36,5	ng/µl	0,913	0,389	2,35	0,23	RNA
1359	31,3	ng/µl	0,783	0,357	2,19	0,1	RNA
1360	76	ng/µl	1,9	0,913	2,08	0,49	RNA
1361	93,6	ng/µl	2,339	1,107	2,11	0,5	RNA
1362	18,3	ng/µl	0,458	0,184	2,49	0,11	RNA
1363-1	119,1	ng/µl	2,978	1,399	2,13	0,66	RNA
1363-2	141,4	ng/µl	3,535	1,691	2,09	0,67	RNA
1364	124,2	ng/µl	3,106	1,476	2,1	0,41	RNA
1365	57,7	ng/µl	1,443	0,684	2,11	0,35	RNA

Supplementary Table 5 (below) shows calculation of normalized values using Myc (test gene) and β-actin (housekeeping gene) data with two different methods.

Table 5. Calculations of normalized values for each sample with Pfaffl method (4th column from the left) and SQ ratio (column on the far right).

	β-ACTIN	MYC		β-ACTIN	MYC	
Sample	Cq Mean	Cq Mean	Pfaffl ratio	SQ mean	SQ mean	SQ ratio (Myc/βact)
164	2,33E+01	2,13E+01	5,96E-03	1,13E+06	3,21E+05	2,84E-01
179	2,90E+01	2,42E+01	2,43E-03	2,34E+04	3,29E+04	1,41E+00
180	2,76E+01	2,53E+01	2,28E-03	5,47E+04	1,40E+04	2,56E-01
181	2,56E+01	2,12E+01	5,04E-03	2,14E+05	3,46E+05	1,62E+00
182	2,65E+01	2,26E+01	3,78E-03	1,48E+05	1,32E+05	8,92E-01
184	2,56E+01	2,03E+01	5,82E-03	2,04E+05	6,86E+05	3,36E+00
189	2,49E+01	2,51E+01	2,93E-03	3,37E+05	1,66E+04	4,93E-02
190	2,47E+01	2,06E+01	5,97E-03	3,94E+05	5,45E+05	1,38E+00
192	2,36E+01	1,94E+01	7,79E-03	1,34E+06	1,36E+06	1,01E+00
1356	2,42E+01	2,55E+01	2,90E-03	5,07E+05	1,26E+04	2,49E-02
1357	2,70E+01	2,35E+01	3,15E-03	8,18E+04	5,56E+04	6,80E-01
1358	2,86E+01	2,41E+01	2,54E-03	2,81E+04	3,74E+04	1,33E+00
1359	2,65E+01	2,51E+01	2,59E-03	1,17E+05	1,71E+04	1,46E-01
1360	2,55E+01	2,52E+01	2,76E-03	2,42E+05	1,56E+04	6,45E-02
1361	2,61E+01	2,51E+01	2,66E-03	1,50E+05	1,66E+04	1,11E-01
1362	2,83E+01	2,36E+01	2,82E-03	3,86E+04	5,30E+04	1,37E+00
1363-1	2,59E+01	2,51E+01	2,69E-03	1,80E+05	1,64E+04	9,11E-02
1363-2	2,61E+01	2,51E+01	2,65E-03	1,50E+05	1,61E+04	1,07E-01
1364	2,65E+01	2,52E+01	2,52E-03	1,13E+05	1,49E+04	1,32E-01
1365	2,74E+01	2,53E+01	2,34E-03	6,35E+04	1,45E+04	2,28E-01

Presented below (in section 9.2), is the RNA extraction protocol, which was edited by Jenni Jouppila in the summer 2017 and used in this thesis for RNA extraction with PAXgene tissue miRNA kit.

9.2 PAXgene® Tissue miRNA Kit Protocol for PE-tissue sections

For isolation and purification of total RNA from tissue samples fixed and stabilized using the PAXgene Tissue System and embedded in paraffin. 2 - 5 sections (5–10 µm) & tissue surface up to 100 mm² can be combined in one sample prep. All steps are carried out at RT (15–25°C) unless otherwise indicated, work in fume hood (until step 17); buffers TR1 and TR2 contain guanidine thiocyanate, which is hazardous if swallowed or inhaled.

Before using the kit for the first time:

1) Prepare 80% ethanol (mixing 24 ml ethanol [96–100%] + 6 ml RNase-free water; supplied)

2) Add 44 ml of ethanol (96–100%) to Buffer TR3

3) Prepare a DNase I stock solution. Dissolve the solid DNase I (1500 Kunitz units) in 550 µl DNase resuspension buffer (RNase-free water). Mix gently by inverting the tube; *do not vortex*. Aliquot and store at –20°C (up to 6 months). Thawed aliquots can be stored at +4°C up to 6 weeks.

Before starting:

- Check buffers TR1. If precipitate has formed, warm to 37°C to dissolve.

- Set the temperature of the heating block (or shaker–incubator, if available) to 45°C

1. Add β-Mercaptoethanol (β-ME) to Buffer TR1 (10 µl β-ME per 1 ml Buffer TM1; in a fume hood!). TR1+β-ME can be stored at RT up to 1 month.

2. Place sections in a 1.5 ml microcentrifuge-safelock tube.

3. Add 650 µl xylene to the sample. Vortex vigorously for 20 s, and incubate for 3 min at RT.

4. Add 650 µl ethanol (96–100%), vortex for 20 s.

5. Centrifuge at maximum speed for 5 min (16 000 *g*).

6. Remove the supernatant by pipetting.

7. Add 150 µl Buffer TR1, and re-suspend the pellet by vortexing 20 s.

8. Add 290 µl RNase-free water, mix. Then add 10 µl proteinase K and mix by vortexing 5 s.

9. Incubate for 15-45 min at 45°C (15 min sufficient when using a shaker–incubator at 1400 rpm; if heating block is used, mix the sample a couple of times during the incubation). Spin down the liquid. Set the temperature of the shaker–incubator to 65°C for use in step 23.

10. Pipet the lysate to a PAXgene Shredder spin column (lilac) placed in a 2-ml processing tube, and centrifuge for 3 min at maximum speed (16 000 *g*).

11. Transfer supernatant of the flow-through fraction to a new 1.5 ml microcentrifuge tube without disturbing the pellet in the processing tube.

12. Add 225 µl ethanol (96-100%). Mix by vortexing for 5 s, and centrifuge briefly (1–2 s at 500–1000 x *g*) to spin down.

Note: The length of the centrifugation must not exceed 1–2 s to avoid pelleting of nucleic acids!

13. Pipet the sample and any precipitate to PAXgene RNA MinElute column (red, in +4°C) placed in 2 ml processing tube. Centrifuge for 1 min 8000 x *g*. Place the spin column in a new 2 ml processing tube. Collect the old processing tube containing flow-through for waste disposal.*

14. Pipet 350 µl Buffer TR2 to the column. Centrifuge for 20 s 8000 x *g*. Place the spin column in a new 2 ml processing tube. Collect the old processing tube containing flow-through for waste disposal.*

15. Make DNase I incubation mix (add 10 µl DNase I stock solution to 70 µl Buffer RDD per to a 1.5 ml microcentrifuge tube supplied with the kit; mix by gently flicking the tube, spin). *Do not vortex.*

16. Pipet the DNase I incubation mix (80 µl) onto the spin column, and incubate for 15 min RT.

17. Pipet 350 µl Buffer TR2 to the column and mix carefully by pipetting up and down 5 times. Centrifuge 20 s 8000 x *g*. Place spin column in a new 2 ml processing tube. Collect the old processing tube containing flow-through for waste disposal.*

18. Pipet 500 µl Buffer TR3 to the column, and centrifuge 20 s 8000 x *g*. Place spin column in new 2 ml processing tube. Discard the flow-through.

19. Pipet 500 µl of 80% ethanol to the column and centrifuge 2 min 8000 x *g*.

20. Discard the processing tube containing flow-through and place the column in a new 2 ml processing tube. Open the cap of the spin column and centrifuge 5 min at max speed.

21. Discard the processing tube containing flow-through. Place the column in 1.5 ml microcentrifuge tube, and pipet 14-40 µl Buffer TR4 directly onto the column membrane. Centrifuge for 1 min maximum speed to elute the RNA.

22. Incubate the eluate 5 min at 65°C to denaturate RNA. After incubation, chill immediately on ice.

23. Store RNA in -80°C long term (-20°C for a couple of days).

*WASTE DISPOSAL:
Buffers TR1 and TR2 contain guanidine thiocyanate, which is collected to a specified container in the fume hood.
***Note**: guanidine thiocyanate can form highly reactive compounds when combined with bleach.
If liquid containing these buffers is spilt, clean with suitable laboratory detergent and water. If the spilt liquid contains potentially infectious agents, clean the affected area first with laboratory detergent and water, and then with 1% (v/v) sodium hypochlorite.